Urban Roadside Tree Inventory Using a Mobile Laser Scanning System

by

Shiqian Wang

A thesis

presented to the University of Waterloo

in fulfillment of the

thesis requirement for the degree of

Master of Science

in

Geography

Waterloo, Ontario, Canada, 2016

AUTHOR'S DECLARATION

I hereby declare that I am the sole author of this thesis. This is a true copy of the thesis, including any required final revisions, as accepted by my examiners.

I understand that my thesis may be made electronically available to the public.

Abstract

Field surveys, as a traditional method for urban roadside tree inventory, is time consuming and labour-intensive, and, therefore, costly. However, more recent technology has allowed a vehicle-borne mobile laser scanning (MLS) system, driving at the speed limits on urban streets, to obtain three-dimensional (3D) georeferenced point clouds with high-density and high-accuracy. 3D MLS point clouds can be used to directly obtain3D information of roadside trees and extract geometrical information such as crown diameter, diameter at breast height (DBH : trunk diameter at 1.3 m height), and tree height. However, a variety of problems make the processing of MLS data very difficult: the large data volume, occlusions, mixed-density and irregular distribution of MLS point clouds as well as complexity of the road environment. Thus, effective methods are needed for the MLS data processing.

The main goal of this thesis is to establish a feasible workflow by testing a series of methods to extract geometrical information of roadside trees from the MLS-acquired point clouds. The workflow developed in this study consists of three parts. The first part deals with ground point removal. As such, only off-ground points are used to extract trees. The second part handles tree detection by comparing four segmentation and clustering methods: the Euclidian distance clustering algorithm, the region growing segmentation method, the normalized cut (Ncut) method, and the supervoxel-based tree detection method. The third part focuses on automated extraction of tree geometric parameters such as tree height, DBH, crown spread, and horizontal slices features. Finally, classification of tree species was conducted using the k-Nearest Neighbour (k-NN) and the random forests (RF) algorithm. A total of four MLS datasets (three in Xiamen, China and one in Kingston, Ontario) acquired in

2013 and 2015, respectively, were used to test the developed method. The ground truthing data of DBH estimation were obtained through manual measurement of selected roadside trees after the two MLS missions in Xiamen in the fall 2015. The field surveyed DBH values of the 163 roadside trees were used to estimate the accuracy of the proposed tree extraction method. The 200 manually labeled trees with 8 different species were selected to examine accuracy of the proposed classification method. The results show that over 90% of the roadside trees were correctly detected, with an average error of about 5% in DBH estimation when compared to the field survey, and an overall accuracy of 78% for the classification of tree species.

Acknowledgements

Firstly, I would like to thank my advisor Prof. Jonathan Li for his guidance on my research and study in the past three years. Prof. Li is very patient and responsible when I make mistakes and feel depressed. I remember he told me, if you are feeling difficulties in your study, it means you are improving. His words guided me through the most difficult time and encouraged me to keep on trying. He can also be very strict when pointing out my mistakes in my thesis. However, I would never finish this thesis without his careful supervision.

I would like to thank the rest of my Thesis Examining Committee: Dr. Derek Robinson, Assistant Professor at the Department of Geography and Environment Management, University of Waterloo; Dr. Michael Chapman, Professor at the Department of Civil Engineering, Ryerson University; and Dr. Yuhong He, Associate Professor at the Department of Geography and Planning, University of Toronto. They spent their precious time to read my thesis and gave insightful comments to make it a better work.

My sincere thanks also go to TULLOCH Engineering for providing the Kingston datasets to support my study. Thanks go to graduate students including Dawei Zai, Zhipeng Cai, Hanyun Wang, and Yongtao Yu from Fujian Key Laboratory of Sensing and Computing for Smart Cities at Xiamen University to help me collect the MLS data, Fan Wu and Huan Luo who helped me with my C++ codes when I worked for hours but still cannot debug them. Finally, I would like to thank PhD students at the University of Waterloo, Jiange Liu, for helping with codes in Matlab and Fan Li for helping with codes in R. I would never be able

to collect the data I need and compile my codes successfully without their intellectual supports.

Although I have been waiting for this day for the past three years and thought I would be very happy when I finish my degree, I found it is hard to say goodbye to these years and the memories. I was lucky to meet my best friends Lanying Wang and Wei Li during my study in Waterloo who were always supportive when I need help. I would also to thank other students: Haochen Zhang, Menglan Zhou, Han Jiang, Weikai Tan, Linfei Ma, Yuenan Li, Xinqu Chen and He Zhao who have created a delightful environment in the office. A special thanks to the visiting scholars in our group including Dr. Min Lu, Dr. Xiaoliang Zou, Dr. Zheng Ji and Dr. Zhiyong Li who have shared their experiences during the group meetings. Finally, I would like to thank the staff of the Writing Centre of the University of Waterloo, who helped improve my English writing.

Last but not the least, I want to thank my family. They supported my study and gave me the courage and faith to go through the stress and difficulties. During the days when I suffered from stomach problems last year, my mother has been taking care of me with great patience. I could not be more grateful for what I got from my parents.

Table of Contents

AUTHOR'S DECLARATION ii
Abstract iii
Acknowledgements v
List of Figures x
List of Tables xii
List of Abbreviations xiii
Chapter 1 Introduction 1
1.1 Motivation 1
1.1.1 Requirements for Urban Tree Inventory 1
1.1.2 Conventional Methods for Urban Tree Inventory 3
1.1.3 Mobile Laser Scanning for Urban Tree Inventory: Challenges 6
1.2 Objectives of the Thesis 9
1.3 Structure of the Thesis 9
Chapter 2 Background and Related Studies 11
2.1 Introduction to MLS 11
2.1.1 Components of a Mobile Laser Scanning System 12
2.1.2 Direct Geo-referencing 13
2.1.3 Comparison of Airborne Laser Scanning 16
2.2 Related Studies 18
2.2.1 Methods for Ground Removal 18
2.2.2 Detection of Individual Trees 20
2.2.3 3D Geometric Measurement 23
2.2.4 Classification of Tree Species 26
2.3 Chapter Summary 31
Chapter 3 Methodology 32
3.1 Study Areas and Datasets 32
3.1.1 Study Areas 32
3.1.2 Datasets 33
3.2 Workflow 37
3.3 Preprocessing 38
3.3.1 Threshold Cut 38
3.3.2 Outlier Removal 39

3.3.3 Ground Removal 40
3.4 Single Tree Extraction 41
3.4.1 Euclidean Clustering 42
3.4.2 Region Growing Segmentation 42
3.4.3 Normalized Cut 43
3.4.4 Supervoxel-based Segmentation 44
3.5 Estimation of Tree Parameters 46
3.5.1 Tree Trunk 46
3.5.2 Tree Crown 47
3.5.3 Tree Height and Width of Cluster 50
3.5.4 Horizontal Percentile Features 51
3.6 Classification 52
3.6.1 Feature Selection 52
3.6.2 Train Classifiers 52
3.6.3 Classification 52
3.7 Accuracy Assessment 53
3.8 Chapter Summary 56
Chapter 4 Results and Discussions 57
4.1 Extraction of Single Trees 57
4.1.1 Threshold Cut 57
4.1.2 Outlier Removal 57
4.1.3 Ground Removal 58
4.1.4 Clustering 60
4.2 Estimation of Tree Parameters 67
4.2.1 Tree Trunk 67
4.2.2 Tree Crown 70
4.2.3 Tree height, SD and Horizontal Slice Features 73
4.3 Classification 73
4.3.1 Feature Selection 74
4.3.2 Classification 76
4.3.3 DBH Estimation 78
4.4 Chapter Summary 82
Chapter 5 Conclusions and Recommendations 84

5.1 Conclusions 84
5.2 Limitations and Recommendations 86
References 89

List of Figures

Figure 1.1: Roadside tree benefits..... 1
Figure 2.1: Components of a typical MLS system (Topcon Positioning System, 2016)..... 11
Figure 2.2: Mathematical modeling for a simple MLS system (Zhang, 2016)..... 14
Figure 2.3: Multi-return of ALS data..... 17
Figure 3.1: Location of Dataset D..... 32
Figure 3.2: Locations of Datasets A, B, and C. 33
Figure 3.3: The RIEGL VMX-450 systems..... 35
Figure 3.4: Four sections in the workflow. 37
Figure 3.5: Illustration of upward growing ground filtering method..... 41
Figure 3.6: Ncut segmentation..... 43
Figure 3.7: Trees Formed by Supervoxels..... 45
Figure 3.8: 2D alpha shape outline extraction method. 48
Figure 3.9: Single tree crown extraction..... 49
Figure 3.10: Horizontal slices of derived tree clusters..... 51
Figure 3.11: The convex hull of a point set. 51
Figure 4.1: Removal of points that are far from the trajectory. (a) MLS data before the threshold cut. (b) MLS data after the threshold cut. 57
Figure 4.2: Outlier removal results. (a) Outliers found in raw MLS data. (b) MLS data after outlier removal. 58
Figure 4.3: Ground removal results. (a) MLS data before ground removal. (b) MLS data after ground removal. 59
Figure 4.4: Ground points removal using 2m global relief..... 59
Figure 4.5: Ground points removal using 10m global relief..... 59
Figure 4.6: Clustering result of Euclidean distance method using Dataset D. (a) MLS data before clustering. (b) MLS data after clustering. 60
Figure 4.7: Clustering results of the Euclidean distance method. (a) Clustering result using a smaller distance threshold. (b) Clustering result using a larger distance threshold..... 61
Figure 4.8: Segmentation results of the region growing method. 63
Figure 4.9: Tree trunk extraction results of the region growing method. 63

Figure 4.10: Segmentation results of the Ncut method. (a) A cluster that was not successfully segmented using the Euclidean distance clustering method. (b) Downscaled high density point cloud. (c) The segmentation result when the method was used to segment connected trees and light poles. (d) The segmentation result when the method was used to segment connected trees. 64
Figure 4.11: Segmentation results of Dataset C using the supervoxel-based method. 65
Figure 4.12: Segmentation results of Dataset B using the supervoxel-based method. 65
Figure 4.13: Segmentation results of connected trees and electricity poles using the supervoxel-based method. 66
Figure 4.14: Errors and undetected trees. 66
Figure 4.15: Extracted tree trunk slices. 67
Figure 4.16Cylinder fit results and problems 68
Figure 4.17 Results of obtained tree centers using the minimum bounding rectangle method. 69
Figure 4.18: Extracted crown outlines using the 2D alpha shape method. 70
Figure 4.19: Results of single tree crown extraction. 71
Figure 4.20: Single tree crown extraction. 71
Figure 4.21: Results of crown diameter estimation. 72
Figure 4.22: Different tree species and a light pole in Dataset C. 74
Figure 4.23: Accuracy and standard deviation for a different number of variables. 75
Figure 4.25: Accuracy for different k values. 77
Figure 4.25: Outlier removal of linear regression inputs. 80
Figure 4.26: Linear regression of DBH using all data inputs (cm). 80
Figure 4.27: Linear regression of DBH estimation. (a)Result of Dataset A using the bounding rectangle method. (b) Result of Dataset B using the bounding rectangle method. (c) Result of Dataset C using the bounding rectangle method. (d) Result of Dataset A using the RANSAC cylinder fit method. 82

List of Tables

Table 1.1: The Instruments and Difficulties for Three Geometrical Measurements in Field Surveys. . 3
Table 2.1: DBH Estimation Methods and Results from ALS and TLS Data. 23
Table 2.2: Tree Height Estimation Using ALS and TLS Data. 25
Table 2.3: Classification Methods and Results of Different Studies. 27
Table 3.1: Datasets. 34
Table 3.2: Error Matrix of Classification of Two Tree Species. 55
Table 4.1: Parameters for Region Growing Segmentation. 62
Table 4.2: Feature Characteristics of Derived Tree Clusters. 73
Table 4.3: Classification Result of Derived Clusters 74
Table 4.4: Importance of Different Variables for Different Class Types 76
Table 4.5: Confusion Matrix of k-Nearest Neighbour Classification. 77
Table 4.6: Confusion Matrix of Random Forest Classification 78
Table 4.7: Overall Accuracy and RMSE for DBH Estimation Using Minimum Bounding Rectangle Method 79
Table 4.8: Regression Results of Different Datasets Using Bounding Rectangle Method And Cylinder Fit Method 81

List of Abbreviations

3D	Three dimensional
ALS	Airborne Laser Scanning
DBH	Diameter at breast height
DBM	Deep Boltzmann machines
DMI	Distance Measurement Indicator
DWT	Discrete Wavelet Transform
EAB	Emerald Ash Borer
ETS	Explicit tree structure
FOV	Field of View
GA	Genetic algorithm
GNSS	Global Navigation Satellite System
GPS	Global Positioning System
IMU	Inertial Measurement Unit
k-NN	k Nearest Neighbours
LDA	Linear discriminate analysis
LiDAR	Light Detection and Ranging
MLS	Mobile Laser Scanning
Ncut	Normalized cut
OA	Overall Accuracy
PCL	Point Cloud Library
RANSAC	Random sample consensus
RF	Random forest
RFE	Recursive Feature Elimination
RMSE	Root-mean-square error
SAR	Synthetic Aperture Radar
SD	Standard Deviation
SVM	Support Vector Machine
TLS	Terrestrial Laser Scanning
TOF	Time-of-flight
VTMR	Variance-to-mean ratio

Chapter 1
Introduction

1.1 Motivation

1.1.1 Requirements for Urban Tree Inventory

In 2050, around 66% of the world's population is expected to live in cities (Roy et al., 2012).This rapid urbanization may result in many urban environmental problems such as poor air quality, dust, noise and urban floods (Islam and Nazrul, 2012).

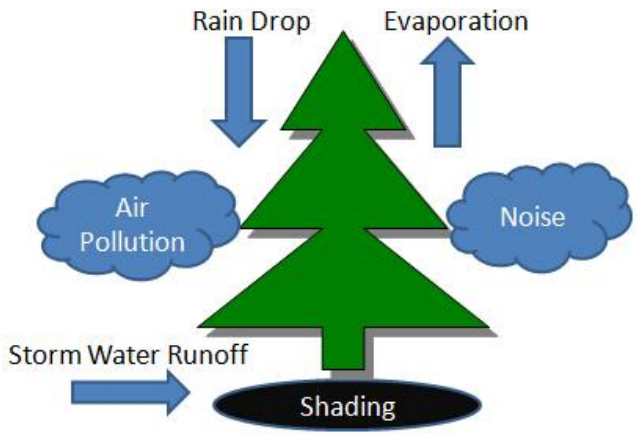

Figure 1.1: Roadside tree benefits

Roadside trees play an important role in solving the above mentioned problems as shown in Figure 1.1. First, trees can help control storm water runoff by interception and infiltration. The soil around trees can absorb water that would otherwise run off the road and tree leaves can prevent rain drops from directly hitting the ground, thus, reducing the runoff

coefficient. Based on a study by Armson et al. (2013), when there are 1m×1m pits around the trees, the runoff coefficient can be reduced by 62% when compared with asphalt. Second, trees can help reduce air pollution and help reduce road noise. Third, trees can adjust the temperature and moisture through shading and evaporation (Roy et al., 2012). However, roadside trees may also have negative impacts. Falling trees or falling tree branches can damage roads and electrical facilities or injure people, especially during storms and on windy days. Planting of the wrong species of trees in urban areas can produce pollen, fruits and seeds that can cause allergies or create road hazards (Pokorny, 2003).

Knowing the geometrical information and tree species of urban trees is important to urban tree protection, urban planning, environmental impact assessment, and tree risks management. For example, geometrical information can help urban planners to determine whether pruning, planting or removal of trees is needed. Tree height and diameter at breast height (DBH) can be used to calculate the biomass of urban trees. Pests like the Emerald Ash Borer (EAB) can cause widespread mortality of ash trees (Villari et al., 2016). Information about tree species and locations can be used to efficiently locate certain tree species when they are infested by pests like the EAB. Moreover, information of tree species may help reduce damage by tree crashes because frangible (i.e., breakable) roadside trees can be planted at places that are more prone to run-off-road accidents (Wolf and Bratton, 2006).

However, urban tree inventories in many cities are often incomplete and inaccurate due to budget problems. Based on a survey conducted in 1980, of 2861 U.S. cities, only 511 cities had information on urban tree inventories (Wood, 1999). Although most of the urban forest data in the U.S. can be found on the Internet, it is mostly derived from air photos and

radar images instead of field surveys. In Canada, only 20% of municipalities have management plans for urban forests, and 25% of municipalities do not have urban tree inventories (Bardekjian, 2016). In China, many of the cities lack the funding and strategies for planning and management of urban forests (Li et al., 2005).

1.1.2 Conventional Methods for Urban Tree Inventory

Field surveys can get most of the information required for an urban tree inventory, such as species, height, DBH, crown spread, soil conditions, tree condition, and location of roadside trees. However, field measurements of DBH, tree height and crown spread are often complicated due to a vast realm of variations within each measurement and confusion when dealing with different trees in different environments (Leverett and Bertolette, 2015). Also, field surveys often require the use of different survey instruments.

Table 1.1: The Instruments and Difficulties for Three Geometrical Measurements in Field Surveys.

Measurement	Instruments	Difficulty
DBH	Tapes, calipers, and monocular	Easy
Height	Rulers, total stations, clinometers and hypsometers	Difficult
Crown Spread	Tapes and rulers	Most difficult

Table 1.1 shows the instruments usually used in a field survey to measure geometrical information about trees such as DBH, tree height, and crown spread. Geometrical information is important because it is often used to define a tree's size and calculate biomass (Leverett and Bertolette, 2015). Calipers and tapes have been used in studies to measure DBH (Saarinen et al. 2014; Thaiutsa et al. 2008). The calipers work better for trees with circular trunks but the tapes work better for non-circular tree trunks. However, the accuracy of the caliper method can be improved by averaging two or more measurements at different angles (Leverett and Bertolette, 2015). Also, the accuracy of the tape method can be affected by the tilt of trees.

The measurement of tree heights is difficult because it is often derived through angle and distance measurements. Angular error, distance error and manual determination of tree tops can affect the accuracy of the height measurement. The accuracy of hypsometers is about 0.45 m to 0.9 m (Leverett and Bertolette, 2015).

The crown spread can be derived by averaging the longest and shortest extent of the crown or using the spoke method which takes more than 10 measurements of crown width from tree trunk to the outer extremities (Leverett and Bertolette, 2015). It is difficult to accurately measure crown spread because the outline of tree crowns cannot be well defined when trees are connected, errors are caused by manually defined tree outlines, blocking of sight, and by estimating the crown spread using the methods based on a few measurements of radius.

To conclude, the advantages of the field survey include high accuracy in DBH measurements, the ability to closely inspect the tree, and a more thorough inventory. For example, information such as soil characteristics, pest hazards and tree species can be easily distinguished. The major problems with field surveys are the cost of labor and time. Also, tree height and crown spread measurements in urban areas can be inaccurate due to tilted tress, limited access to trees, and blocking of sight. Moreover, tree position is often represented by street names and sequential numbers in a field survey (Wood, 1999). Thus, they cannot be directly registered to a GIS database, therefore, make locating a certain tree time consuming.

Aerial photos have been used for urban tree inventories. Interpretation of aerial photos has three advantages: (1) easy access of datasets (2) easy estimation of crown diameters and tree positions, and (3) simple implementation. However, visual interpretation of digital aerial images may require professional knowledge to identify different tree types (Kätsch and Kunneke, 2006). Although colour infrared imagery can be used to distinguish vegetation from other objects, human errors may cause trees to be misclassified or omitted. Also, the accuracy of such methods highly depends on the pixel size of the image, and tree trunks cannot be seen from these images.

To derive tree height information from images accurately, Kätsch and Kunneke (2006) used a stereo photogrammetric method. They also claimed that, although DBH cannot be directly derived from the images like tree crowns, it can be derived from crown diameter using analytical methods. Their method can estimate tree heights with an accuracy of ± 0.5 m, and the DBH estimation's overall accuracy was around 90%.

Satellite images have been used to help build tree inventories. Although vegetation can be separated from other objects in these images in leaf-on seasons, some tree species that share similar spectral reflection characteristics cannot be well classified. Also, these images are often affected by weather conditions and cloud coverage (Walton et al. 2008).

Synthetic Aperture Radar (SAR) imagery has often been used for tree inventory due to the radar's ability to work in all kinds of weather situations. Tree height can be derived based on SAR interferometric techniques such as repeat–pass or single-pass interferometry. However, some small trees' crown spread cannot be derived because the limited resolution of the SAR imagery (e.g., 2.5 m × 3.2 m) (Garestier et al., 2011). Also methods based on backscatter intensities cannot establish the relationship between intensities with DBH and tree height (Garestier et al., 2011).

The map-based approaches like the Open Tree Map make it possible for people to edit urban tree maps in an interactive geographic information system (GIS) application. People can record the trees they planted by mapping the tree on the Open Tree Map. Also, programs like the 'Green Street Canada' send equipment to community members to involve them in urban tree inventory. However, the accuracy of the data cannot be confirmed (Morneau, 2005).

1.1.3 Mobile Laser Scanning for Urban Tree Inventory: Challenges

With the fast development of Light Detection and Ranging (LiDAR) technology, studies of tree classification and information extraction using LiDAR data have become a hot topic in fields of computer graphics and remote sensing. Unlike 2D imaging systems such as

the optical and radar images discussed before, LiDAR systems can obtain 3D information about objects precisely by sending and recording laser beams.

In an Airborne Laser Scanning (ALS) system, the laser scanners are mounted on an aircraft. Most ALS companies suggest that the accuracy for height estimations is 15 cm in root-mean-square error (RMSE), but it can be affected by different scan heights and topographies. ALS data have been used for many forestry applications such as biomass estimation and tree species classification. For example, Vainio (2009) showed an RMSE of 18% for biomass estimation using ALS data. Reitberger (2008) classified trees into two clusters (coniferous, deciduous) and received an overall accuracy of 85% in a leaf-on situation. These studies show that MLS can obtain high accuracy for biomass estimation and can separate coniferous and deciduous trees with high accuracy. Methods such as full waveform analysis and intensity analysis are often used in tree species classification. However, the DBH of trees is often modeled based on tree heights in these studies.

Compared with ALS, Mobile Laser Scanning (MLS) data is used less in the study of forestry due to some of its limitations: smaller coverage, larger data volume, and higher price. Thus, most studies using MLS focus only on extracting man-made objects such as buildings, roads, and utility facilities; vegetation near the road is often ignored. With the fast development of MLS technology, new MLS systems are becoming cheaper, more accurate, and more widely used. Thus, MLS provides the potential for simultaneously extracting tree information during road surveys to help update current roadside tree inventories.

Since the laser scanners are mounted on a vehicle in an MLS system, the major advantages of MLS data are better point density on trees and a direct view of tree trunks. However, the point density of MLS data varies over the distance from the laser scanners to roadside trees. As such, those trees far from the scanners may not be well represented. Another problem is the large volume of MLS data. In the MLS data used in this study, for example, a 100 m road section may consist of over 3 million points, which makes the processing of such data difficult and time consuming. The representation of point clouds is also a challenge when compared with images. Since points are scattered in 3D space without a regular structure, the algorithms that can be easily applied to images such as neighbour search and feature extraction may face a greater challenge when applied to MLS data. Finally, the classification of tree species using point clouds can be difficult due to the lack of spectral information. For example, Brandtberg (2007) reported on classification results with an overall accuracy of 64% for three tree species: oak, red maple, and yellow poplar using MLS data recorded in leaf-off conditions.

Terrestrial Laser Scanning (TLS) can obtain higher point density than MLS and can be placed in high density forests where vehicles cannot go. However, the ground plan estimation of TLS can be difficult due to occlusions of terrain surfaces and tree trunks (Matthew et al. 2012). Also, it is difficult for TLS to cover large areas because moving TLS systems is not as efficient as MLS systems.

1.2 Objectives of the Thesis

Using MLS for urban roadside tree inventory is still a new research topic compared with ALS-based forestry studies. Therefore, it is important to analyze the limitations and accuracy of MLS for improving urban tree inventory. The major research objective is to establish a feasible workflow for automated tree species classification and extraction of tree location, crown diameter, DBH, and tree height. Some of the specific objectives are:

(1) To test the efficiency and errors of the outlier removal method and the voxel-based ground removal method.

(2) To compare four different segmentation and clustering methods and develop a method that can segment individual trees, especially connected trees for MLS datasets.

(3) To compare two different classification methods using different combinations of input information.

(4) To assess the accuracy of the proposed DBH estimation method using field survey data and test the accuracy of the proposed classification method using manually labeled data.

1.3 Structure of the Thesis

This thesis consists of five chapters. Chapter 1 introduces three key aspects: the motivations, challenging problems, and objectives of the study.

Chapter 2 explains the background of the study and related studies using ALS, TLS, and MLS.

Chapter 3 presents the methods used to extract 3D information about roadside trees and classify tree species. In each stage of the workflow, one or more methods are tested and discussed to choose the best one to be applied in the study.

Chapter 4 presents and discusses the results for each method tested in the study using figures and tables. The validation result of the proposed methods is also included.

Chapter 5 draws the conclusions, discusses the limitations, and makes future research suggestions.

Chapter 2
Background and Related Studies

This chapter introduces the components a MLS system and the principle of direct georeferencing. Since methods developed for ALS are adjusted for use in this study, a comparison of MLS and ALS is included in Section 2.1.3. Section 2.2 provides the literature review of related studies using MLS, ALS and TLS data.

2.1 Introduction to MLS

Figure 2.1 shows the components of an MLS system. An MLS system is an integrated platform consisting of four parts: one mobile platform, one or more laser scanners, a high precision positional system, and one or more digital cameras (Puente, 2013).

Figure 2.1: Components of a typical MLS system (Topcon Positioning System, 2016)

2.1.1 Components of a Mobile Laser Scanning System

(1) Mobile Platform

The mobile platform can be a boat, a train or a car that carries the laser scanners and other components (Puente et al., 2013). The control system is often located in the front seat where people can adjust the scan mode and observe data output. The moving speed of the platform should be adjusted to obtain sufficient point density.

(2) Range Measurement Components

Two types of laser scanners can be used to measure range: the time-of-flight (TOF) method and the phase shift method. The TOF scanner can calculate the range by sending a short laser pulse to the target and record the time for the emitted pulses to return to the receiver. The range 'R' is calculated by the following expression:

$$R = \frac{1}{2} c\Delta t \tag{2.1}$$

where c is the speed of light and Δt is the TOF of the pulse (Puente et al., 2013).

In contrast, phase shift laser scanners use the phase difference between the emitted and received backscattered signal to determine the range. The range measurement of phase shift laser scanners is more accurate, but the measurement range is shorter (Puente et al., 2013).

(3) Positioning Components

Three types of technologies are used in the positional system to determine the position of a mobile vehicle: satellite positioning by a Global Navigation Satellite System

(GNSS), inertial navigation using an Inertial Measurement Unit (IMU), and a Distance Measurement Indicators (DMI). The positional information of an MLS platform and the IMU is often updated by GPS and GNSS (Guan, 2013). At places where the GPS and GNSS signal are deteriorated by high-rise buildings and tunnels, the IMU and DMI units can observe the moving distance, acceleration, roll, pitch, and heading of the vehicle to update the positioning information (Guan, 2013).

(4) Digital Cameras

Digital cameras are often mounted on the top of the vehicle to take videos or colour images of the surveyed area simultaneously with laser scanning. These videos and digital images can be used to produce true color point cloud data or provide image representation of the surveyed area (Williams et al., 2013).

2.1.2 Direct Geo-referencing

The direct geo-referencing technique makes it possible for MLS systems to produce instant coordinate information for each recorded point. Some of the positional information such as the distance and angle between the IMU, laser scanner and GPS is provided by the manufacturer, but other positional information that cannot be measured directly needs to be calculated based on measurable vectors using geometrical relations (Barber et al., 2008).

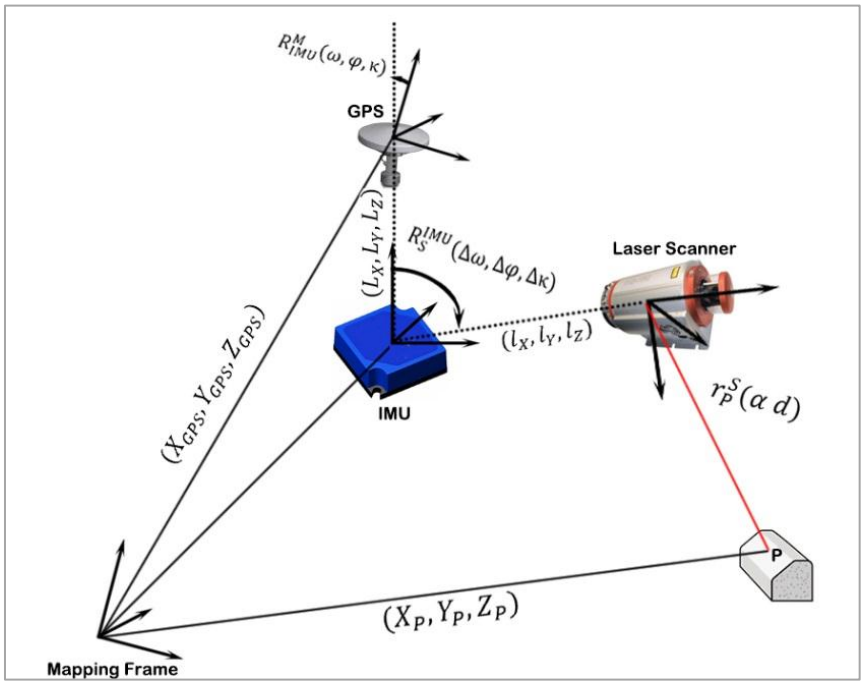

Figure 2.2: Mathematical modeling for a simple MLS system (Zhang, 2016)

Figure 2.2 shows a typical MLS system in which, the location of the target P in the mapping frame can be derived by the following equation (Barber et al., 2008).

$$\begin{bmatrix} X_P \\ Y_P \\ Z_P \end{bmatrix}^M = \begin{bmatrix} X_{GPS} \\ Y_{GPS} \\ Z_{GPS} \end{bmatrix}^M + R^M_{IMU}(\omega,\varphi,\kappa) \cdot \left(R^{IMU}_S(\Delta\omega,\Delta\varphi,\Delta\kappa) \cdot r^S_P(\alpha,d) + \begin{bmatrix} l_X \\ l_Y \\ l_Z \end{bmatrix}_S^{IMU} - \begin{bmatrix} L_X \\ L_Y \\ L_Z \end{bmatrix}_{GPS}^{IMU} \right) \quad (2.2)$$

where

X_P, Y_P, Z_P are the coordinates of the target *P* in the mapping frame.

$X_{GPS}, Y_{GPS}, Z_{GPS}$ are the coordinates of the GNSS antenna in the mapping frame.

$R^M_{IMU}(\omega,\varphi,\kappa)$ is the rotation matrix between the IMU and mapping frame,$(\omega,\varphi,\kappa)$are the roll, pitch and yaw of the sensor with respect to the local mapping frame. These values are provided by the IMU system.

$R_S^{IMU}(\Delta\omega, \Delta\varphi, \Delta\kappa)$ is the rotation matrix between the laser scanner and IMU, $(\Delta\omega, \Delta\varphi, \Delta\kappa)$are the boresight angles which align the scanner frame with the IMU body frame. These values are determined by the system calibration.

$r_P^S(\alpha, d)$ is the relative position vector of Point P in the laser scanner coordinate system, α and d for scan angle and range measured and returned by the laser scanner.

l_X, l_Y, l_Z are lever-arm offsets from the IMU origin to the laser scanner origin.

L_X, L_Y, L_Z are lever-arm offsets from the IMU origin to the GPS origin. These lever-arm offset values can be determined by system calibration or physical measurements.

Nowadays, the development of high quality positioning hardware and mathematical models has improved positioning accuracy. Positioning errors of MLS systems mainly arise from multi-path effects and signal shading caused by high-rise buildings and trees along the street can sometimes deteriorate the GPS signals in a moving vehicle (Haala et al. 2008).Thus, the IMU and DMI are used to help obtain positional information in places with poor satellite coverage (Williams et al. 2013). The constant drift rate of IMU may also cause positioning errors. However, the constant drift rate of IMU in mobile systems has dropped from 0.003 degrees per hour to 0.0005 degrees per hour in recent years (Schwarz and Sheimy, 2007). The measurement of the lever- arm offset can be measured indirectly using physical measurements or calibration methods which may also cause errors due to uncertainties when aligning the laser scanner axes and the IMU axes (Wang, 2016).

2.1.3 Comparison of Airborne Laser Scanning

In this section, the RIEGL LMS-Q560 scanner employed in the study by Reitberger et al. (2008) is selected as an example of ALS scanners. The RIEGL VMX-450 scanner employed in this study is used as an example of MLS scanners. The scanners are compared from three aspects: point density, coverage, accuracy, and field of view (FOV).

(1) Point Density

The point density of MLS and ALS data can be affected by pulse frequency, scan distance, and the speed of the moving platform. The average point density of the ALS data is 25 points/m ^{2} at 400 m flying height, which is much lower than that of the MLS data. The point density in ALS data is nearly the same because the change of distance between objects and the scanner is relatively small when compared with the long scan range. However, the point density in MLS data varies with distance to the trajectory. The MLS data used in this study's average point density on ground surface near the trajectory is around 3000 points/m^2, but the average point density for trees far from the trajectory is only around 300 points/m^2.

(2) Coverage

Although the MLS systems' maximum scan range can reach 140 – 220 m, objects far from the scan trajectory often have low point density or are occluded by buildings, trees, cars, and the ground. By contrast, the coverage of ALS is determined by the flying height and scan angle. With a scan angle of 22.5 ^{o} and a scan height of 400 m, the swath of the ALS is about 160 m.

(3) Accuracy

Errors with MLS and ALS can arise from positioning measurements, angle measurements, calibration errors, multipath effects, and range measurement errors. The large scan range of ALS leads to uncertainties and larger footprints. Based on the data provider, the accuracy of the MLS is 8 mm at a scan range of 50 m, and the accuracy of the ALS is 20 mm at a scan range of 250 m.

(4) View

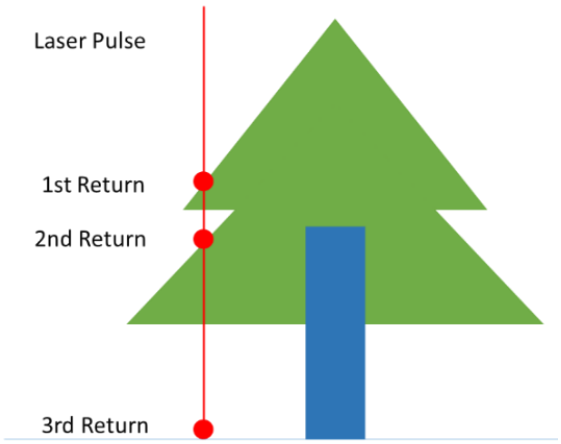

Figure 2.3: Multi-return of ALS data.

The FOV of MLS is a side view whereas ALS has a top view of trees. Thus, tree trunks are often estimated by models based on tree height or crown spread for ALS data. However, multi-return, as shown in Figure 2.3, makes tree layer analysis easier for ALS data. Since the laser beam is assumed to hit different layers of tree structures before hitting the ground, the multi-return waveform can be used for tree species analysis (Holmgren and

Persson, 2004). Full-waveform analysis can be difficult for MLS because clear layers may not be found in the scan direction.

To conclude, the ALS and MLS data are 3D points with information such as their coordinates, intensity, return numbers, time and scan angle. The accuracy of MLS is higher than ALS, but the coverage of MLS is smaller. Using MLS for tree species classification can be challenging but the estimation of DBH can be easier and more accurate.

2.2 Related Studies

The use of ALS data in forestry inventory has been well studied in the past decades (Yao et al. 2016). Although MLS data have a higher density and direct view of tree trunks, challenges such as data volume, occlusions, and coverage make it is less used in forestry studies. In an attempt to address this gap, this thesis introduces an adjusted method that can be applied to MLS data for single tree information extraction and classification. This section begins by introducing current methods used for ALS data and TLS data in order to discuss their suitability as MLS data. This is followed by conclusions about the methods reviewed.

2.2.1 Methods for Ground Removal

Since a large proportion of MLS points are ground points, their removal can improve the processing speed and facilitate later processes. The process of ground removal is similar to generating DTM from point clouds but the interpolation of derived ground points is not needed. Generating DTM from ALS data has been well studied by researchers to facilitate forestry analysis, hydrology analysis, and geological hazard control (Razak et al. 2013). Most of the ground filtering algorithms for ALS are based on slope, interpolation, morphological

filters, and hybrid methods (Maguya et al., 2013). The hybrid methods combine slope, interpolation and other algorithms to enhance the filtering performance. However, some of these methods may not work well for MLS data due to the different scale of the data. For example, the morphological filters, such as opening and closing, require the rasterizing of point cloud data, which may lower the accuracy of derived ground models (Pingel et al., 2013). Opening and closing is the combination of two fundamental operations in the morphological filters: dilation and erosion. Dilation uses vector addition of set elements to connect two sets and erosion uses the vector subtraction of set elements to combine two sets (Haralick et al., 1987).

Moskal and Zheng (2012) applied a slope-based method to remove ground points from the raw TLS data. First, the slope-based method divides the data plot into square voxels. Voxels are regular elements in 3D space and the word voxel comes from the combination of vox ("volume") and el ("element") (Foley et al., 1990). The method compares the slope between adjacent points in each voxel with a pre-defined slope threshold. Specifically, the higher point will be considered a non-ground point when the slope is larger than the threshold. However, the slope-based method performs poorly in steep terrain. Also, some of the off-terrain objects that are below the defined slope threshold can be misclassified as ground points (Wang, 2016).

Some interpolation-based methods, such as the Triangular Irregular Network (TIN), the Kriging interpolation method, and the linear prediction method, extract ground surface based on the assumption that the terrain surface is smooth (Maguya et al. 2013). These methods work well in large scale datasets but may not be suited for individual tree analysis.

Also, some of the interpolation-based methods compute all points to estimate terrain relief (Wang, 2016). However, the lower time efficiency of such methods will become a problem for a large volume TLS or MLS data.

Yu et al. (2015 b) proposed an efficient upward growing method for ground filtering of MLS data. First, the method voxelizes the dataset to enhance the time efficiency of the algorithm. Then, the method searches 9 upward voxels for the lowest voxels until it cannot find 9 upward voxels on top. Finally, the height of the cluster and height difference between clusters and the global lowest point are used to separate grounds points and non-ground points. The method can perform well in places with uneven grounds and also distinguishes between terrain surface and small vegetation. However, the method does not work well in steep terrain. Wang (2016) reported an accuracy assessment of this method and received the RMSE around 9 cm for the derived DTM.

To conclude, raster-based methods can lower the accuracy of derived ground points and interpolation-based methods may not work for MLS data due to the large volume. Thus, the upward growing method was applied in this study.

2.2.2 Detection of Individual Trees

After the ground points are removed from the data, individual trees are often extracted to obtain crown diameter and intensity of each single tree.

Vosselman et al. (2004) have reviewed many point cloud segmentation methods. However, many of the methods such as scan line segmentation, surface growing segmentation and 3D Hough transform are based on segmentation of planes and lines.

However, such features may not be found in tree clusters. Although some of the trees can be detected from their cylinder trunks, conifer trees and trunks covered by leaves can be difficult to locate. A similar problem occurs when using the surface normal based method proposed by Ioannou et al. (2012). Firstly, the method can compute a point's surface normal from its neighbour points. Secondly, the normal difference of two points is computed. Finally, the clusters can be segmented using the magnitude threshold. The advantage of this method is its ability to segment objects in different scales including cars and pedestrians (Ioannou et al., 2012). However, the result may cause missing tree points and may bring up errors in tree species classification and tree information extraction.

Some of the segmentation methods require the rasterizing of point cloud data. For example, Dalponte and Bruzzone (2011) used averaging height and intensity in each grid to rasterize the ALS data. A region growing segmentation method that can automatically locate seed points was applied to the raster Dataset. Yao et al. (2012) also rasterized the ALS data before applying a watershed segmentation method. Similar to the region growing method, the grids that have the local maxima height were defined as tree positions. Then, the edges of each watershed were defined by elevation of pixels. Interpolating the point clouds to raster datasets can allow image segmentation methods to be easily applied to the point cloud data, but problems such as mixed pixels, interpolation and empty pixels will reduce the data accuracy. Also, small trees that grow under big trees or grow near big trees are often neglected in these methods (Yao et al., 2012).

Some other researchers have combined alternative data with point clouds to extract trees. Dinuls (2012) combined multispectral data with ALS data to identify individual trees

after tree tops were found using a crown height model. However, registration of different data types will involve geo-correction processes and may produce errors.

Yu et al. (2015) claimed that the Normalized Cut (Ncut) method can be used for separating connected trees. First, this method uses voxels to represent the Datasets. Then, voxels pairs' similarities are computed to group points that belong to one object. By maximizing the similarities in each segment and minimizing the similarities between different segments, the lower trees can also be segmented (Yao et al. 2012). Although the method works well for separating different trees, the iteration of finding voxel pairs makes it very time-consuming, and consumes too much computer memory space because all weight matrices have to be stored during the clustering process. Also, users have to define the number of clusters that should be segmented. Thus, this method was applied after the first segmentation method based on the study of Yu et al. (2015) and Yao et al. (2012).

Yu et al. (2015) recommended a Euclidean distance clustering method for efficient tree extraction using MLS data. The method can cluster points based on the points' Euclidean distance to its neighbours based on a user defined distance threshold. However, setting the threshold for the method can be difficult because a small distance threshold may lose tree points and a large threshold cannot segment close objects. To define the suitable distance threshold, the average distance between adjacent points needs to be manually observed. The optimal distance threshold was found by adjusting different values around the average distance. This method is compared with the region growing segmentation method, the Normalize cut method, and the supervoxel-based tree extraction method in this study to extract single tree clusters.

2.2.3 3D Geometric Measurement

After single trees are extracted from point clouds, 3D geometric information such as DBH, crown diameter and tree height can be calculated. This information is usually used for biomass estimation and classification of tree species.

(1) DBH

Table 2.1: DBH Estimation Methods and Results from ALS and TLS Data.

Data Type	Point Density	Single Tree Extraction Method	DBH Estimation Method	RMSE (cm)	Reference
ALS	25 pts/m2	Watershed	Least squares adjustment	5	Yao et al. (2012)
TLS	NA	NA	Cylinder fitting and least squares method	9.17	Moskal and Zheng (2011)
	NA	NA	Cone fitting	13.1	McDaniel et al. (2012)
	NA	NA	Cylinder fitting	13.2	

Table 2.1 shows some of the methods used for DBH estimation using both MLS and TLS data. Since tree trunks cannot be seen directly from ALS data, models have been used to estimate the DBH based on other features. For example, Yao et al. (2012) used a least squares adjustment to estimate DBH using field survey data and features such as tree height, crown area, crown volume and crown height. The result shows that the R^2 is around 0.7, the relative RMSE is around 15% and the RMSE is around 5 cm. Yao et al. (2012) also determined that the estimation for conifer trees is more accurate than deciduous trees.

The side FOV of MLS and TLS makes a direct estimation of DBH for roadside trees possible. Since point density on tree trunks may not be enough for circle fitting, tree trunks are often sliced horizontally into cylinders. Moskal and Zheng (2011) used a least-squares method to fit a cylinder model using sliced trunks from TLS data. Their DBH estimation's RMSE was 9.17 cm. McDaniel et al. (2016) also applied the least-squares method to fit a cylinder model and then compared it with a cone model. He also compared the error difference between two data inputs: tree trunks and trunk slices. The result shows that the cone model received best results when the tree trunks were used in the fitting; the two methods worked much the same when using trunk slices. However, the estimation of DBH for non-circular trunks using this method can be a problem. Thus, the cylinder fit method is compared with a proposed minimum bounding rectangle method in this study.

(2) Tree Height

There are two ways to extract tree height using point clouds as shown in Table 2.2. Reitberger et al. (2008) used the height difference between highest tree points and the height of DTM to represent the height of trees. However, errors in DTM will affect this estimation. Moskal and Zheng (2012) and Lin et al. (2014) used the height difference between highest tree points and lowest tree points to estimate tree heights. Their estimation's RMSE is around 0.75 m when compared with field survey. However, Moskal and Zheng (2012) revealed that although the point density of TLS is very high, the laser beam cannot penetrate tree leaves and reach tree tops, causing underestimations of tree heights. Also, the underestimation of tree heights can be caused by occlusion at lower parts of tree trunks by bushes and grass. Although Lin et al. (2014) suggest that their estimation of tree height achieved a very high R^2,

the results were compared with tree height estimation based on TLS data. However, manually extracted tree clusters may enhance the estimation accuracy.

Table 2.2: Tree Height Estimation Using ALS and TLS Data.

Data Type	Point Density	Single tree extraction	Height estimation	Accuracy	Reference
ALS	12 pts/m2	Image based	DTM based	$R^2 = 0.69$; mean standard error = 1.1 m	Brandtberg et al. (2003)
TLS	N/A	N/A	Single tree cluster based	$R^2 = 0.573$; Standard error = 0.75 m	Moskal and Zheng (2012)
MLS	N/A	Artificially identified	Single tree cluster based	$R^2 = 0.94$	Lin et al. (2014)

To enhance the efficiency of the algorithm, DTM of the study area was not generated and the single tree cluster based height estimation method was applied. However, occlusion of second row trees may cause trouble for height and DBH estimation in the MLS data.

(3) Crown Spread

Some of the studies that focus on estimation of stem volume such as Moskal and Zheng (2012) use canopy cover to represent the tree crown without extracting single tree crowns. However, the estimation of above ground biomass can be affected by individual tree crown diameter estimation (Kankare et al. 2013). Actually, 78% of the biomass variance can

be explained by crown diameter alone and the crown diameter can enhance the accuracy of the estimation of biomass for 0.24 in R^2 and 7 t/ha in RMSE (Kankare et al. 2013).

Many studies have estimated the single tree crown diameter to enhance biomass estimation accuracy. For example, Rutzinger et al. (2008) used enclosing circles to represent crown diameter at different heights. However, some of the trees with irregular crowns cannot be well represented by circles. Thus, some of the studies calculate the crown diameter by averaging the long side and short side of the crown. However, some of the trees in the MLS data have irregular crowns; thus the spoke method mentioned in the field survey methods is used to calculate crown diameter. Kwak et al. (2010) claimed that the estimation accuracy of crown diameter can be affected by stand density. The RMSE of their study is 0.63 m for low density plots, and 1.11 m for high density plots. This difficulty is also found during the process of MLS due to the segmentation problem of dense vegetation.

2.2.4 Classification of Tree Species

During the past two decades, many researchers have pointed out that tree species classification is one of the most important tasks for tree inventory (Dinuls et al., 2012).Multispectral and hyperspectral images have been used for tree species classification and received highly accurate results. However, using point clouds alone for tree species classification is still a challenging task.

Table 2.3: Classification Methods and Results of Different Studies.

Data Type	Point density (pts/m^2)	Feature selection	Classification	Tree Types	Overall accuracy	Reference
ALS	25	N/A	K-means	2	85.4% (Leaf-on)	Reitberger et al. (2007)
ALS	N/A	Student's t test	LDA	2	95%	Holmgren and Persson (2004)
ALS	90	GA	LDA	4	77.50%	Li et al. (2013)
MLS	250 to 500	DBM	SVM	10	86.10%	Guan et al. (2015)
TLS	N/A	N/A	SVM	4	77.50%	Lin and Herold (2016)
TLS	N/A	N/A	RF	5	88%	Othmani et al. (2013)

Table 2.3 shows the studies that use different types of data and methods to classify tree species. Reitberger et al. (2008) used the K-means classifier to conduct an unsupervised classification of deciduous and coniferous trees. They used a curve to fit the laser waveform data and the results show that the decomposition of waveform received a better classification result than the method that used only the first and last returns in leaf-on situations. The advantage of such method is that less human labeling work is needed.

Holmgren and Persson (2004) combined geometrical, intensity and full-waveform features in the classification of spruce and pine trees using ALS data. This study examined a number of inputs: (1) relative median height, (2) 10% height percentile, (3) 90% height percentile, (4) the relative standard deviation of heights, (5) the mean vertical distance between first and last return of the double pulse, (6) the proportion of single returns, (7) the

proportion of second returns, (8) crown shape parameters, and (9) mean intensity, maximum intensity and mean surface intensity. These features were selected based on a student t test, and both linear classification and quadratic classification were used in the study. The linear classification received better classification results in most of the plots and its overall accuracy of the two species classification was 95%.However, the classification in one of the plots was only 75% because many spruce trees under the pine trees were not detected. Also, the misclassification of tree species can be explained by the variation among tree species (Holmgren and Persson, 2004).

Dalpone and Bruzzone (2011) used a data fusion method that combines hyperspectral data with point clouds to classify different tree species. They indicated that hyperspectral data can help detailed classification and analysis of similar forest types and enhance the classification of tree species by 1% to 4% in kappa accuracy using SVM classifier.

Since the full-waveform analysis of MLS cannot represent the horizontal features of a tree, Guan et al. (2015) used tree structures to represent the waveform. First, the method cut the single tree point cloud into n horizontal slices. Second, the point number in each slice, instead of the intensity value in a full-waveform analysis for MLS data, was used to build a waveform to represent tree profile. Finally, a Deep Boltzmann Machines (DBM) feature generation model and the SVM classifier were applied in the classification process (Guan et al. 2015). The classification achieved an overall accuracy of 86.1% for ten different tree species.

A similar study was done by Li et al. (2013), who used Variance-To-Mean Ratio (VTMR) to represent tree features in each horizontal slice. When the VTMR is smaller than 1, the points are dispersed; when the VTMR is bigger than 1, the points in that slice are clustered (Li et al., 2013). The Genetic Algorithm (GA) was then used for feature selection. Finally, a Linear Discriminate Analysis (LDA) classifier was used and the final classification's overall accuracy was 77.5%.

The advantages of using TLS data for tree species classification are the high point density and the ability to do multi-scans at different directions. Most studies suggest that higher point density can lead to better classification results (Li et al. 2013). Different from most of the MLS scanning data, the multi-scan of TLS data can record points on different sides of a tree by doing scans from different directions. For example, Lin and Herold (2016) used one scanner and Othmani et al. (2013) used two different scanners to do the multi-scan and received high density point clouds from two different views.

Lin and Herold (2016) proposed an innovative classification method that uses Explicit Tree Structure (ETS) feature parameters as input parameters. The ETS feature parameters use derived geometrical information to describe tree characteristics such as tree stem, branch, crown and leaf. In a study by Othmani et al. (2013), the point density of the TLS data allowed 3D triangular meshes of tree trunks to show the texture of different tree trunks. A Discrete Wavelet Transform (DWT) was applied to the texture data to extract the trunk features. Lastly, a Random Forest (RF) classification method was used and obtained an overall accuracy of 88% for five different trees.

In conclusion, (1) high density point clouds can provide more details and enhance classification accuracy. It was reported that classification studies using 0.5–20 points /m ^{2} data showed around 10–20 % less accurate than studies using>40 points /m ^{2}data (Li et al., 2013).

(2) Feature selection methods are important for classification. First, an increase in features may decrease the model's generalization ability and introduce noises. Second, the features may increase the computational time of classification (Dalponte and Bruzzone, 2011). Thus, different kinds of feature selection methods were applied to enhance the classification accuracy. The advantage of the GA method is its global optimization capability and its ability to find an optimal solution based on just a part of the feature space (Li et al., 2013). The student's t test, which is a correlation based feature selection method, can find features that best suit the classification in each correlated feature group (Holmgren and Persson, 2004). The advantage of the DBM method is its ability to produce high level feature representation for high dimensional data.

(3) Different kinds of classification methods have been used in different studies but the majority of the studies used supervised classification methods. The advantage of SVM is its ability to classify high dimensional feature space; however, the interpretability of SVM is still a problem (Pal, 2009). However, RF produces a clear classification tree and it can classify unbalanced data and data with missing values (Pal, 2005). Also, the RF method requires less parameter input than SVM (Pal, 2005). Since features extracted from 3D laser points are unbalanced in a 3D feature space and there may contain missing values in the training set, the RF method was chosen as the classification method.

(4) Detailed classification of tree species can be more difficult than classification of two different types. Classification of trees species that share similar geometrical features can be difficult for low density point cloud data. Also, trees of different ages can represent different features and cause problems for classification.

2.3 Chapter Summary

This chapter focused on the background and related studies of using laser scanning data for tree extraction and classification. Principles of laser scanning technology and differences between ALS and MLS were introduced first. Then, methods that were used in related studies were compared and discussed. Four conclusions were presented: (1) some methods that focus on large scale topography may not work for MLS; (2) voxelization of point cloud data can enhance the processing speed for large volume MLS data; (3) extraction of a single tree is important for generating accurate single tree parameters; and (4) the selection of features can affect the classification accuracy of tree species.

Chapter 3
Methodology

This chapter begins with the description of the study areas and the datasets used in the experiments including the structure of the datasets and the device used for acquiring and processing the MLS data. Also, the measurement of reference data is included. The methods concerned are presented in three parts: the extraction of single trees, estimation of tree parameters, and classification of tree species. Finally, the validation methods are presented.

3.1 Study Areas and Datasets

3.1.1 Study Areas

Figure 3.1: Location of Dataset D.

Figure 3.1 shows the location of Dataset D, which is in the city of Kingston, Ontario, Canada. Kingston is a northern city with many conifer trees and the roadside trees have different heights and variety of sizes

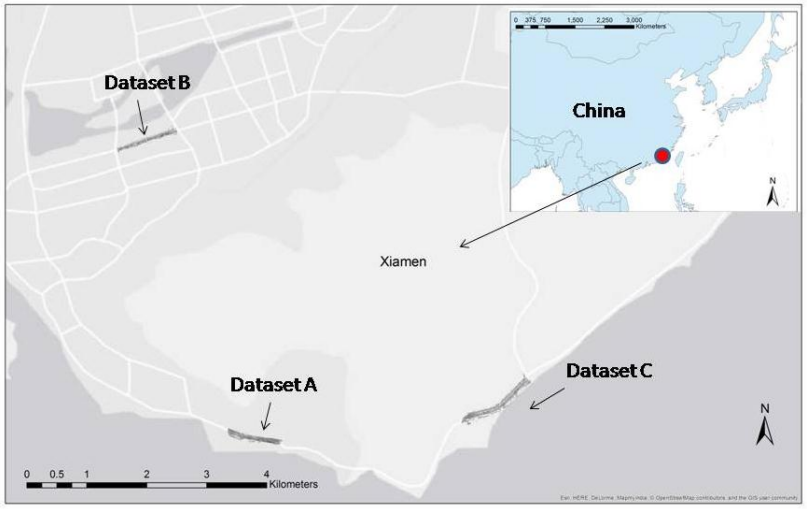

Figure 3.2: Locations of Datasets A, B, and C.

Figure 3.2 shows the location of Datasets A, B, and C, in the city of Xiamen, Fujian, China. Xiamen is a coastal city where the roadside trees are dense and contain a lot of tropical plants. The crowns of these tropical plants are smaller and the wide variety of roadside trees in the datasets can be used to test the classification algorithms.

3.1.2 Datasets

To test the proposed method and algorithms, a total of four MLS datasets were used (see Table 3.1). The first three Datasets A-C were collected by a RIEGL VMX-450 system from Xiamen University in Xiamen and Dataset D was provided by Tulloch Engineering, also using a RIEGL VMX-450 system.

Table 3.1: Datasets.

	Dataset A	Dataset B	Dataset C	Dataset D
Tree types	2	1	7	NA
Tree density	Scattered	Closely arranged	Scattered	Closely arranged
Time	2013/11/25	2015/8/20	2015/9/12	2013/8/21
Road width (m)	25	30	35	25
Road length (m)	1200	1000	500	500
Scan type	One-way	One-way	One-way	Two-way
Point density (pts/m^2)	4000	1000	1000	8000
Vehicle speed (km/h)	50	50	50	25
Location	Huandao Road South, Xiamen	Hubing Road South, Xiamen	Huandao Road East, Xiamen	Kinston

Dataset A is the simplest one with only two types of trees planted at wide intervals. However, a large number of cars, pedestrians, light poles, road signs and bus stops in Dataset A cause occlusions of tree trunks. Trees in Dataset B were planted close to each other with high grasses and shrubs near the tree trunks, making the segmentation of individual trees difficult. These two datasets were used for geometrical information extraction.

Dataset C with seven different kinds of trees was used for both geometrical information extraction and testing of classification methods. Some of the tree species with similar shapes were difficult to classify.

Dataset D was used to test segmentation methods and the geometrical information and tree species information were not extracted. The dataset is characterized by the high point density and large conifer trees near the road. Some of the conifer trees' trunks are not

exposed, making it difficult to estimate their DBH directly. Also, the trees in Dataset D have a larger range of sizes.

(a) (b)

Figure 3.3: The RIEGL VMX-450 systems.

Figures 3.3 (a) and 3.3 (b) show the RIEGL VMX-450 systems used to collect MLS Datasets in Xiamen and Kingston respectively. These two systems have two full-view RIEGL VQ-450 laser scanners, two GPS units, four CS-6 digital cameras, one IMU mounted on the rear top of the vehicle, and one DMI installed on the left rear wheel. The positioning accuracy of this system is 8 mm based on the information provided by the manufacturer (RIEGL, 2015). As can be seen from Figure 3.3, the two VQ-450 laser scanners were symmetrically mounted on top of the vehicle on both left and right sides. The systems can do 400 scans and capture 1.1 million measurements in one second and four photos in different directions are taken every second (RIEGL, 2015).

Although the datasets were acquired by the same type of VMX-450 systems, the point density varies from one dataset to another due to the moving speed of the vehicle, road width and times of survey. The point density in Dataset A is lower than that of Dataset C due to the width of the road. Since road width in Dataset B is the smallest, only the data from one scanner was acquired to reduce the data volume. The point density in Dataset D is also very high due to the two directional survey of the area. Also, the average speed of the platform is around 50 km/h for the Datasets A, B, and C in Xiamen and around 30 km/h in Dataset D, Kingston. The driving speed of the platform can also affect the pattern of derived point clouds. For example, points in Datasets A, B, and C have a larger interval between adjacent scan lines in the direction of the scan trajectory. The pattern may influence the performance of cylinder detection methods using trunk slices.

After the data are recorded by the MLS system, the organization of the Datasets can be important for further processes. To organize the derived point clouds, an LAS file was chosen for outputting data from the software provided by RIGEL because the reading speed of the LAS file is very fast and the file size is small. After the data is divided into smaller scenes, it can be loaded onto a laptop with a 3.89 GB usable memory and a 2.5 GHz processor. The PCD data format was adopted due to its ability to record classified and organized point cloud data and to store data of different types.

To get reference data, 156 trees' DBHs were recorded during the field work using steel rulers and soft rulers for Dataset A, B, and C. First, the steel ruler was used to measure the 1.3 m height. Then, a soft tape was used to measure the DBH. The smallest unit of the ruler and the tape were 1 mm. Errors in the breast height measurement mainly come from the

soft soil problem and the tilt of the ruler. Errors may also arise from curved tape and tilted trees. Also, photos from four digital cameras were used to distinguish different tree species.

3.2 Workflow

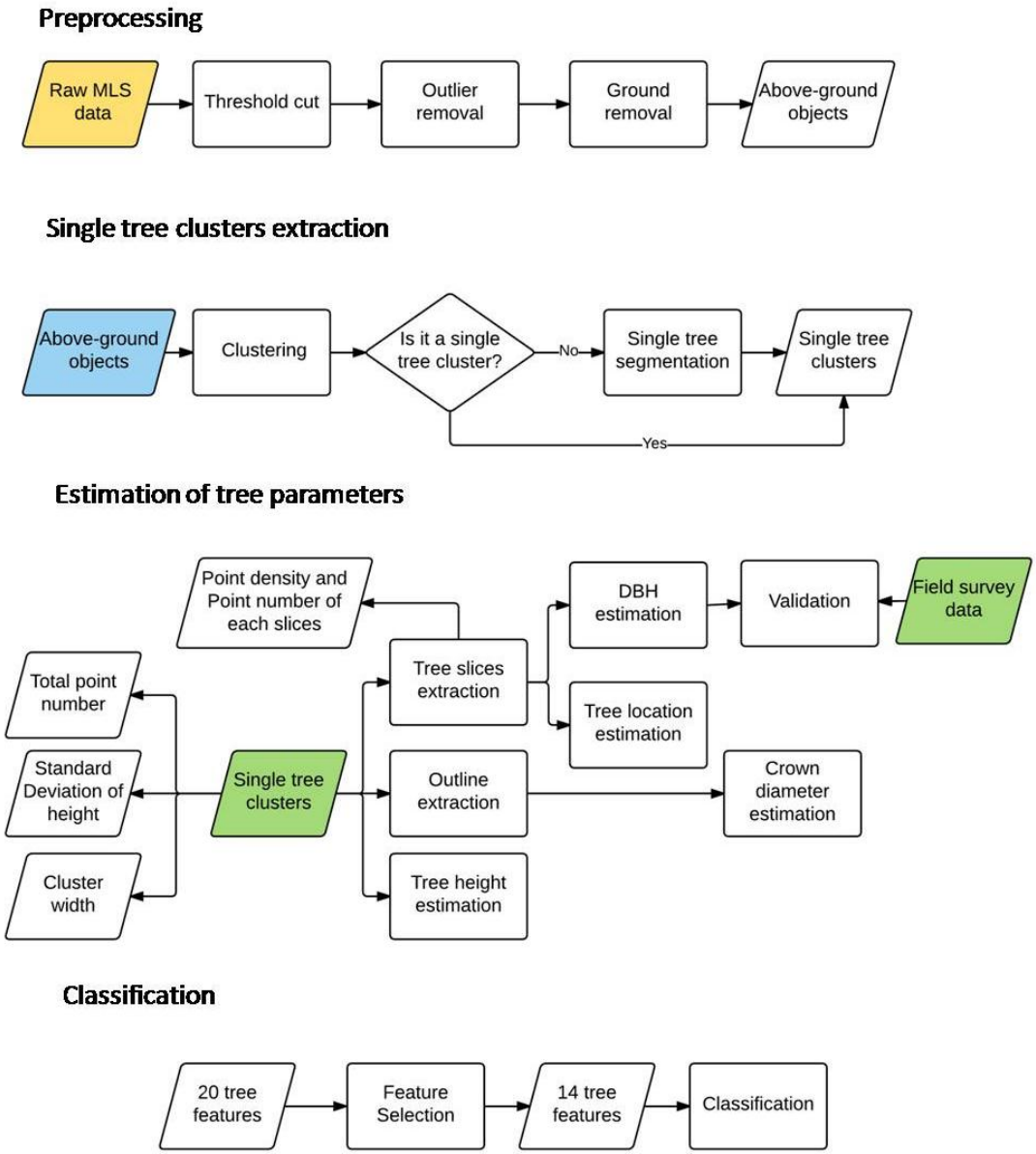

Figure 3.4: Four sections in the workflow.

As shown in Figure 3.4, the entire workflow can be divided into four parts: (1) extraction of single trees, (2) estimation of tree parameters, (3) tree species classification, and (4) validation. During the process of single tree extraction, three different methods were tested and compared: Euclidean clustering, Ncut, and region growing segmentation. After the tree clusters were extracted, a 2D alpha shape method was used to obtain cluster outlines. The Random Sample Consensus (RANSAC) fitting method and a bounding rectangle method were used for calculating DBH. Then the parameters such as tree height, total point number, point density and point number for each height percentile, and standard deviation (SD) of point height were applied to the classification method. After using the Recursive Feature Elimination (RFE) method to select relevant features, two different classifiers, k-NN and RF were applied. In this study, Datasets C and D were chosen since they have more tree species. Finally, the estimation of DBH and tree species classification was validated. A more detailed explanation of the workflow will be included in the following sections.

3.3 Preprocessing

3.3.1 Threshold Cut

Since MLS data cannot accurately capture objects that are far from the scanning trajectory because of point density and occlusion problems, the pass-through filter from PCL can be used to remove redundant data that are far from the trajectory. As a result, only trees that are near the trajectory are included in the study.

3.3.2 Outlier Removal

The raw MLS data always have many error points that are not on the surface of objects, often called outliers or noise measurements, which can be caused by GPS or IMU errors and multipath reflections (Lopera and Lerma, 2014). For example, the location of the vehicle can produce significant errors when the GPS signal is unstable, and the laser receivers may record reflected signals from other objects before the real reflection reaches the receiver.

Outliers can cause problems when the data are processed because these points can lead to erroneous changes in surface normal, point coordinates, and curvatures. Thus, a statistical outlier removal filter from Cloud Compare (Version 4.5, 2016) was used to remove some of the outliers. First, the method computes distances of all points' k-NN. Then, the global mean distance and standard deviations of the distances are calculated. Finally, points with a mean distance to their k-NN that exceeds the interval defined by the global mean and standard deviation are removed from the data (PCL, 2015). The default setting of the threshold is:

$$d_{max} = d_a + n * sd \tag{3.1}$$

where d_{max} is the threshold, d_a is the average distance, sd is the standard deviation of the average distance, and n is the multiplier. Different n values were tested and it was set as 10 to make sure no tree points were removed. Clustered outliers were removed manually.

3.3.3 Ground Removal

Around 60% of the points in the raw Datasets are ground points and these points can cause segmentation errors of tree clusters. Thus, the ground points were removed from the datasets using an upward growing ground filtering method to enhance the efficiency and accuracy of segmentation.

Figure 3.5 shows a simple example of the upward growing ground filtering method. Similar to pixels in images, a voxel represents a 3D grid in the MLS data. First, the point clouds are cut into regular rectangular grids parallel to the X-Y plane to simplify the discrete points and store topological information in the row number and column number. Second, the method searches nine upward neighbour voxels for the bottom voxels until it cannot find nine upward neighbour voxels (Yu et al., 2015). The green voxel in Figure 3.5 is selected as a seed voxel, and the blue voxels represent the nine upward voxels that are searched. The height difference between the lowest point in the bottom voxel and the highest point in the top voxel is defined as H_l. The height difference between the lowest point in the bottom voxel and the lowest point in the data scene is defined as H_g. Finally, if the H_l is smaller than the local terrain relief and H_g is smaller than the global terrain relief, the voxel clusters are classified as ground points (Yu et al., 2015). The local terrain relief can be defined by the fluctuation of ground surface. Since the ground in the study area is almost flat, the local terrain relief was set as 0.3 m. The global terrain relief can be defined by the height difference between the lowest ground point and the highest ground point in the datasets. For areas with significant elevation changes, the global terrain relief was set as 10m; for places with small elevation changes, the global terrain relief was set as 2 m.

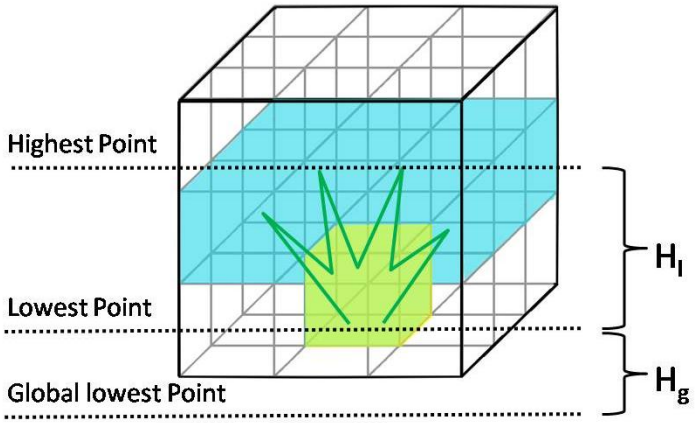

Figure 3.5: Illustration of upward growing ground filtering method.

This method was applied in this study because it is very efficient, simple to use, and capable of dealing with small fluctuations on the road. However, the method cannot be used in areas that have a large slope surface because the global lowest point in the area cannot accurately represent the ground elevation in such areas. Also, error points that have a lower height than ground surface have to be removed from the dataset before the data can be filtered using this method.

3.4 Single Tree Extraction

After redundant data are removed from the Datasets, clustering methods can be applied to separate each single tree. Setting thresholds of cluster size can also help remove small clusters such as grass and shrubs. Two methods were tested in this study: the Euclidean clustering method and the region growing segmentation method.

3.4.1 Euclidean Clustering

First, the input point clouds were stored in a Kd-tree structure to facilitate the nearest neighbour search (Yu et al., 2015). Second, for each point *p* in the Dataset, the neighbour points whose Euclidean distance from point *p* were within a user-defined radius were extracted. The extracted points that were not processed were added to a queue waiting to be processed. When all points in the queue were processed, the points in the queue could be stored in a cluster. Third, the algorithm finishes when all points are set to their own cluster and all points in the dataset are processed. Finally, clusters that fit certain criteria were labeled as tree clusters.

Four parameters need to be set during this process: the node number *k*, which will affect the leaf size; the distance threshold that defines the neighbour search radius; the height threshold of derived clusters to remove grass and shrubs; and the point number threshold to remove small noisy clusters. However, the distance between points in a tree cluster can be large in places with fewer leaves and thin trunks. The method achieved unsatisfactory results for some of the datasets.

3.4.2 Region Growing Segmentation

The region growing segmentation is often used to cluster points that form a smooth surface. First, the curvatures of all points in the Dataset are calculated using the nearest neighbours around each point. Points with the lowest curvatures are selected as seed points. Second, the angle difference between the seed points and their neighbour points is calculated. When the difference is smaller than the angle threshold set by the user, the points are added

to the cluster. Third, the neighbour points that have smaller curvatures than the defined curvature threshold are added to the seed list, and the original seeds are removed. Last, when the seed set is empty, the algorithm begins from the start (PCL, 2015).

3.4.3 Normalized Cut

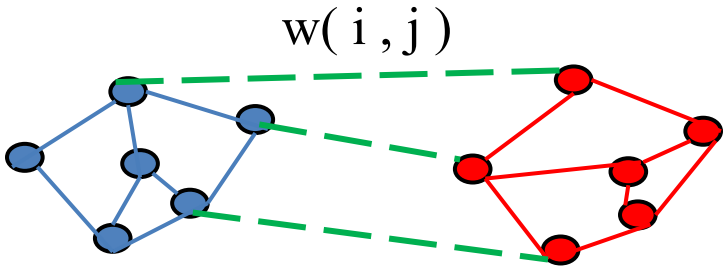

Figure 3.6: Ncut segmentation

Figure 3.6 shows the example of two point clusters (the red dots and the blue dots) and the cutting weight between point pairs (the green lines). Firstly, the MLS was divided into a voxel structure. Secondly, the nonempty voxels were selected and the similarities among each pair of voxels were computed by (Yu et al., 2015):

$$w_{ij} = \begin{cases} \exp\left(-\frac{\left\|p_i^{XY}-p_j^{XY}\right\|_2^2}{\sigma_{XY}^2}\right) * \\ \exp\left(-\frac{\left|p_i^{Z}-p_j^{Z}\right|^2}{\sigma_Z^2}\right), \ if \ \left\|p_i^{XY}-p_j^{XY}\right\|_2 < d_{XY} \\ 0, otherwise \end{cases} \tag{3.2}$$

where $p_i = (x_i, y_i, z_i)$ and $p_j = (x_j, y_j, z_j)$ are the centroids of voxels i and j. $p_i^{XY} = (x_i, y_i)$ and $p_j^{XY} = (x_j, y_j)$ are the coordinates of the centroids on the X-Y plane, $p_i^Z = z_i$ and , $p_j^Z = z_j$ are the z coordinates of the centroids. σ_{xy} and σ_Z are the standard deviations. d_{XY} is the

maximum threshold of the horizontal distance between two voxels. The centroid of voxel *i* is defined as follows:

$$p_i = \frac{1}{N_i}\sum_{m=1}^{N_i} p_m^i \tag{3.3}$$

where N_i is the total number of points within voxel *i* and p_m^i is a point within voxel *i*.

Thirdly, the method divided the point cloud into groups by maximizing the similarities in each group and minimizing similarities between different groups using the following equation:

$$\text{Ncut(A,B)} = \frac{cut(A,B)}{assoc(A,V)} + \frac{cut(A,B)}{assoc(B,V)} \tag{3.4}$$

where $cut(A,B)$ is the total sum of weights between voxel groups *A* and *B*, and $assoc(A,V)$ is the sum of the weights of all edges ending in voxel group *A*.

The minimized *Ncut(A,B)* is derived by solving the generalized eigenvalue problem (Shi and Malik, 2000):

$$(D - W)y = \lambda Dy \tag{3.5}$$

where *D* is a diagonal matrix with $D(i, i) = \sum_m w_{im}$.

3.4.4 Supervoxel-based Segmentation

Figure 3.7 shows an example of generated supervoxels. These supervoxels can be generated using the Voxel Cloud Connectivity Segmentation method. A voxel can be transformed into a supervoxel by assigning properties such as the geometrical center of the

voxel, mean laser reflectance intensity value of constituting 3D points, and surface normals (Aijazi et al. 2013). After the supervoxels were extracted, they were projected to the X-Y plan and a convex hull was used to represent their area. Information such as the highest point, lowest point, bounding box, and gravity center of the super voxels was also extracted (Wu, 2016). The coordinates of the gravity center were calculated by:

$$x = \frac{\sum_{i=1}^{n} x_{pi}}{n}$$

$$y = \frac{\sum_{i=1}^{n} y_{pi}}{n} \tag{3.6}$$

where p_i belongs to the supervoxel, n is the number of points in the supervoxel (Wu, 2016).

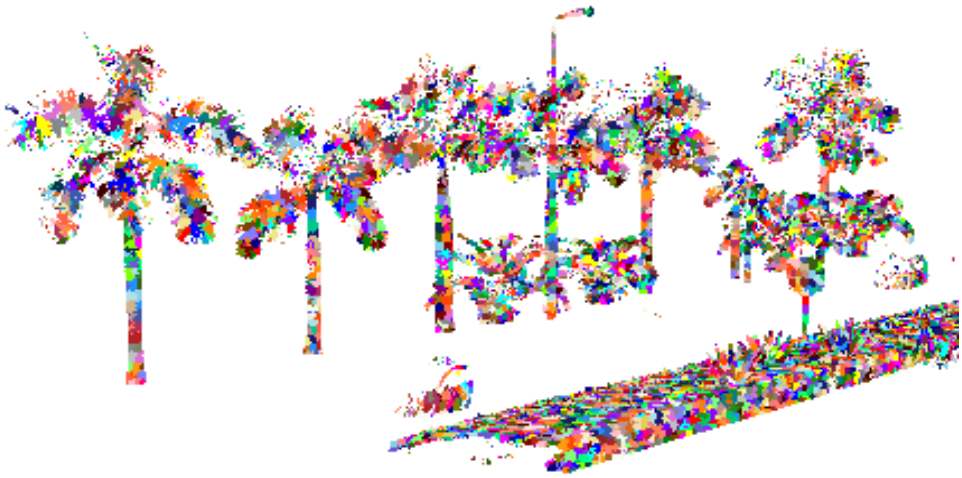

Figure 3.7: Trees Formed by Supervoxels.

Firstly, the highest local points were extracted. Secondly, supervoxels near the local highest points were considered trunk voxels. Thirdly, trunk voxels that have a highest point below a user-defined threshold were removed. This threshold should be higher than the average bush height of the area. Finally, the neighbour voxels of extracted voxels were examined using distance thresholds. The complete tree cluster was derived by growing both upward and downward.

3.5 Estimation of Tree Parameters

3.5.1 Tree Trunk

A threshold cut method was used to cut the tree clusters so as to extract tree trunks,. For Dataset B, the height filter was set as 0.9 m to 1.1 m; for Dataset A and C, the height filter was set as 1.2 m to 1.4 m because the trees in Dataset B started to branch at a height of around 1m. The *z* value of the lowest point in each cluster was found first followed by that the points of selected range of height were extracted. The height of the horizontal slice of a trunk was defined by the point density of the data to get enough points for the RANSAC shape detection method.

(1) Cylinder Fit

To find the location of the tree centre and DBH from the trunk slices, the RANSAC cylinder detection method was applied firstly. The pre-assumption of the fitting is that the other side of the tree trunk that cannot be seen from the MLS data is mostly symmetrical to the side that can be seen from the street. This method was used because the points on a tree

trunk can be described as a cylinder model when the height of the trunk is cut small. First, the method randomly selects minimum points that are required by the model from the Dataset. The model parameters are calculated based on the selected points. Second, other points that fit the model up to a certain threshold are considered a "consensus set". If the number of points in the consensus set exceeds the number of the minimum support points defined by the user, the model is recorded as a good one. The maximum iteration time was set as 1000 and the model that receives the most support points is considered the best one.

(2) Minimum Bounding Rectangle

However, some of the trees in Dataset B have twisted trunks that cannot be detected with a cylinder fit function. A minimum bounding rectangle method was proposed to solve the problem of non-cylindrical tree trunks in Dataset B. The method assumes that the centres of minimum bounding rectangles are also the centres of tree trunks when half of the symmetrical tree trunks are captured by MLS data. Firstly, the method uses a minimum bounding rectangle center to represent the tree trunk center. Then, it computes the average distance from the center point to outline points as the tree trunk radius.

3.5.2 Tree Crown

(1) 2D Alpha Shape Outline Extraction

Since most of the tree crowns are spread in the X-Y plane, the clusters of trees are projected to the X-Y plane to represent their crown shape in a plane. Firstly, the Z coordinate values of the clusters were set as zero. Since only the outline of the cluster is needed for crown estimation, a 2D alpha shape representation of the tree crowns was introduced. The

method can work better than a convex hull because some of the trees have irregular crown shapes that cannot be accurately represented by convex hulls.

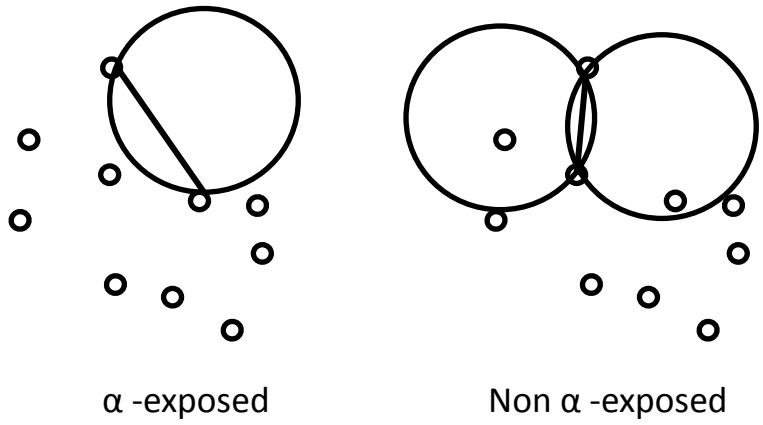

Figure 3.8: 2D alpha shape outline extraction method.

The alpha shape here can be described as a linear approximation of the original shape of the tree crown captured by MLS data. As can be seen from Figure 3.8, the method can determine whether a point is exterior or interior by testing if there is an empty circle that contains no other points. Edelsbrunner and MÄucke (1994) provided the example of carving ice-cream that contains chocolate pieces to illustrate the idea of the method. The radius of the sphere-formed ice-cream spoons is the defined alpha value; a smaller alpha value will allow us to carve more ice-cream without hitting chocolate pieces. The triangles and line segmentation remaining after the carving are the 2-D alpha shape of the space.

(2) Segmentation of Crown Outline

Although the derived outline can represent single tree crowns for single tree clusters, some of the clusters in Dataset B have 2 to 5 trees that still need segmentation. However, the

crowns of these trees overlap with each other and it is hard to determine to which tree the points belong. The Ncut method can separate connected trees but the method is not efficient and the connected trees have to be manually extracted. Thus, this thesis proposes a simple distance-based method that can automatically cut the crown outlines to single crown outlines.

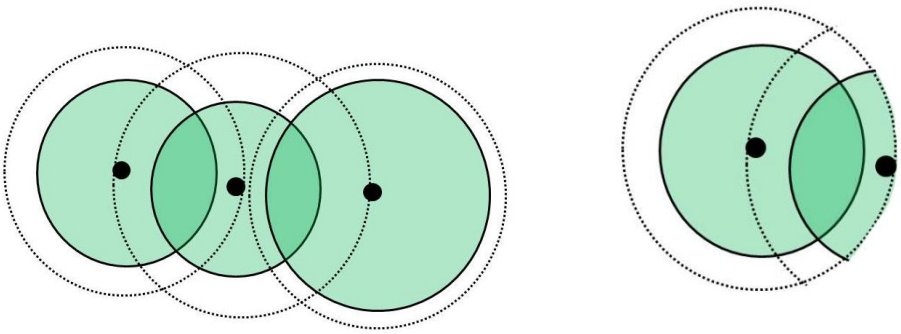

Figure 3.9: Single tree crown extraction.

The method requires the use of the trunk location data derived in the previous DBH estimation process. First, the method finds the trunks within the cluster to determine how many trees are clustered. Second, the method calculates the average distances between each trunk and its adjacent trunks as D_{max}. Thirdly, the largest distance D_{max} is used to cut the cluster outline into different parts. Figure 3.9 shows how the method extracts outline points that are within the distance D_{max} for one of the trunks, in which the black points represent trunk positions, and the dash line represents the threshold D_{max}. Although this method cuts more points not belonging to the trunk, the RANSAC circle detection method (which will be introduced later) can find the crown diameter using some of the outline points.

However, the method assumes that the trees have circular crowns with similar diameter and are planted at similar distances from each other. Thus, the method may not work for other datasets where the distance of two tree trunks is much smaller than their crown diameter.

(3) Crown Diameter Estimation

After the trees are separated from each other, the outline points that were extracted from the 2D alpha shape method were used to get tree crown diameter. The RANSAC shape detection method was used to extract the crown diameter for trees with a rounded crown. For trees with an irregular crown, the crown spread is derived by the spoke method, in which the distances from outline points to the trunk centre are calculated followed by using the average value to represent the crown diameter.

3.5.3 Tree Height and Width of Cluster

The tree height is derived by finding the height difference between the highest and the lowest point in the single tree cluster. Also, the SD of each height data is calculated. The x-width is represented by the largest X coordinate difference, and the y-width is represented by the largest Y coordinate difference.

3.5.4 Horizontal Percentile Features

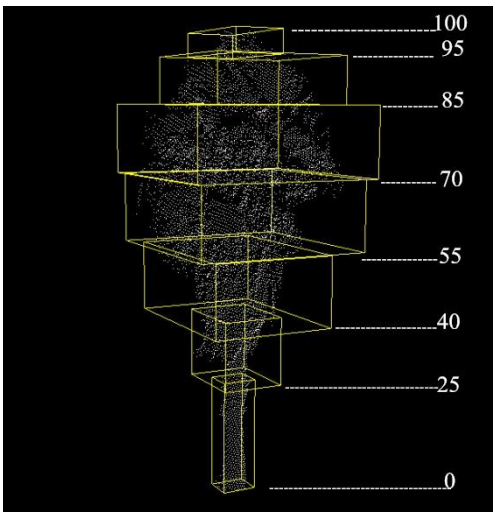

Figure 3.10: Horizontal slices of derived tree clusters

As can be seen in Figure 3.10, 95, 85, 70, 55, 40, and 25th percentile are selected to cut the tree clusters into horizontal slices in this study. For each slice, two different parameters are calculated: the point density and point number. Firstly, the 2D convex hull of each horizontal slice was extracted to compute the area of the slice.

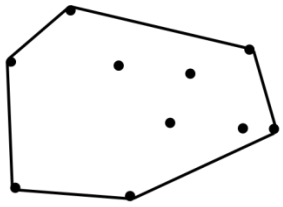

Figure 3.11: The convex hull of a point set.

As shown in Figure 3.11, a convex hull, the smallest convex set that encloses the point cloud in its Euclidean plane, can be used to represent the area of the horizontal slice. Andrew's monotone chain convex hull algorithm was applied to extract the convex hull of the derived slices. Finally, the point density of each slice is computed by:

$$Pd = \frac{Pn}{A} \quad (3.5)$$

where, P_d is the point density of the slice, P_n is the number of points in the slice, and A is the area of the convex hull of the slice.

3.6 Classification

3.6.1 Feature Selection

Since some of the derived features may produce noise, a Recursive Feature Elimination (RFE) method was applied to enhance the classification accuracy. The goal of RFE is to select features by recursively considering smaller and smaller sets of features. First, the estimator is trained on the initial set of features and weights are assigned to each one. Then features whose absolute weights are the smallest are pruned from the current set features. The procedure is recursively repeated on the pruned set until the desired number of features to select is eventually reached.

3.6.2 Train Classifiers

After the tree features are extracted from the clusters, manual labeling of tree species is needed to generate training samples. 52 trees were selected as training samples from the 206 data inputs.

3.6.3 Classification

(1) k-Nearest Neighbour

Given a query point x_i, the k-NN method can find the k training points x_j, $j = 1, 2\ldots, k$ that are closest in distance to x_i, where k can be defined by the user (Meng and Cieszewski,

2007). x_j can be classified using the majority vote among its *k*-nearest neighbours or the weighted average of its k nearest neighbours (Meng and Cieszewski, 2007).

The method is compared with the RF method because it is relatively easy to implement.

(2) Random Forest

Firstly, the RF method randomly samples the input data to generate a group of classification or regression trees. Secondly, the method iterates several times and outputs the best classification result using the vote of each decision tree (Hudak et al., 2008). The advantage of the RF method is that it achieves a more robust model than single classification trees (Hudaket al., 2008). Also, the generalization error can converge and solve the over fitting problem when the number of trees increases because of the Strong Law of Large Numbers (Pal, 2005). Since the input tree features have many uncertainties and some of the trees have fewer samples, the RF method was chosen as the classification method.

3.7 Accuracy Assessment

(1) DBH

After the DBH was estimated, the results were compared with field measurements. A linear regression method was applied to improve the estimation accuracy. The method can model the relationship between estimated values and reference data by estimating the unknown model parameters in the linear predictor functions. Three parameters are calculated to evaluate the regression model: overall accuracy, RMSE, and the R^2, which is the

coefficient of determination of the regression model that can represent how well the model fits the data. The R^2 is calculated by:

$$R^2 = \frac{SS_R}{SS_T}$$

$$SS_T = \sum_i (y^i - \bar{y})^2, SS_R = \sum_i (\hat{y} - \bar{y})^2 \quad (3.5)$$

where y^i and $\hat{y}$ are the original data values and estimated values respectively, $\bar{y}$ is the mean of the observed data (Hedge Found, 2016).

The overall accuracy of the DBH estimation is obtained by:

$$\text{Overall accuracy} = 1 - \frac{|\sum De - \sum Dr|}{\sum Dr} \quad (3.6)$$

where $\sum Dr$ is the total value of reference DBH for the selected cross validation Datasets and $\sum De$ is the total value of the estimated DBH. The RMSE is calculated by:

$$\text{RMSE} = \sqrt{MSE} \quad (3.7)$$

$$\text{MSE} = \frac{\sum_{i=1}^{n} (De - Dr)^2}{n} \quad (3.8)$$

where *MSE* represents the mean square error, *n* is the number of measurements, D_e is the estimated DBH value, D_r is the reference DBH value.

(2) Classification

The accuracy of the classification is represented by a confusion matrix, one of the most widely used accuracy assessment methods (Wang, 2016). Table 3.2 shows an example

of binary classification. T_p is the true positive value that represents the numbers of tree 1 that are classified correctly, F_n is the false negative value that represents the numbers of tree 1 that are misclassified as tree2, F_p is the false positive value that represents the numbers of tree 2 that are misclassified as tree 1, T_n is the true negative value which represent the numbers of tree 2 that are classified correctly.

Table 3.2: Error Matrix of Classification of Two Tree Species.

	Predicted		
Actual		Tree 1	Tree 2
	Tree 1	T_p	F_n
	Tree 2	F_p	T_n

The classification results of this study were evaluated using three criteria: overall accuracy, completeness, and correctness. The overall accuracy can be derived by:

$$\text{overall accuracy} = \frac{\text{Tp+Tn}}{\text{Tp+Tn+Tp+Tn}} \tag{3.9}$$

The completeness of the classification was calculated by

$$\text{completeness} = \frac{\text{Tp}}{\text{Tp+Fn}} \tag{3.10}$$

Correctness was obtained by

$$\text{correctness} = \frac{\text{Tp}}{\text{Tp+Fp}} \tag{3.11}$$

3.8 Chapter Summary

This chapter introduced the proposed methodology for MLS-based urban tree inventory. Firstly, the study area and data of the study were presented. Secondly, the preprocessing methods such as outlier removal, ground removal and threshold cut were discussed. Thirdly, methods for single tree cluster extraction were compared. Fourthly, 3D information extraction was introduced. Then, features were selected using the RFE method, and the two classifiers, RF and k-NN were discussed. Lastly, the methods for accuracy assessment of DBH estimation and tree species classification were explained. The outlier removal and threshold cut was accomplished using the Cloud Compare (Version 4.5, 2016) software. R (Version 3.2.2, 2016) was used for classification and SPSS was used for accuracy assessment and regression analysis. The ground removal algorithm was provided by Yu et al. (2015), and the other codes were developed using Visual Studio 2012 based on algorithm libraries such as the Point Cloud Library (PCL) and the Computational Geometry Algorithms Library (CGAL).

Chapter 4
Results and Discussions

4.1 Extraction of Single Trees

4.1.1 Threshold Cut

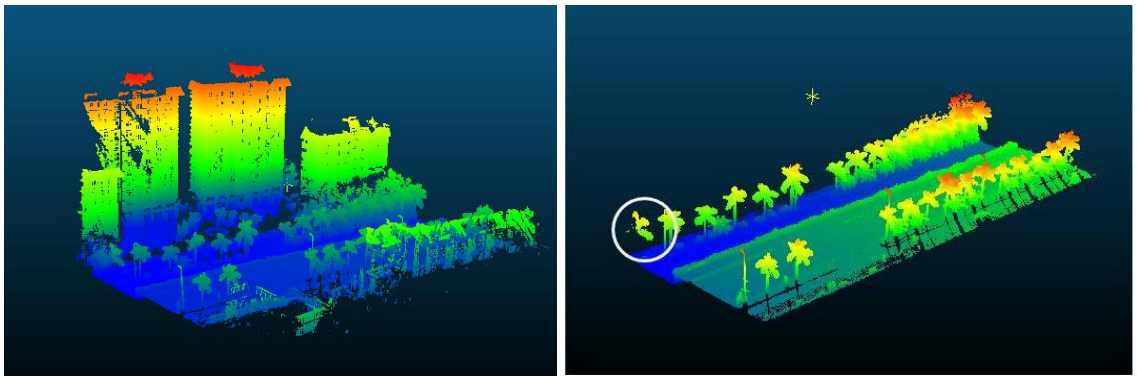

(a) (b)

Figure 4.1: Removal of points that are far from the trajectory. (a) MLS data before the threshold cut. (b) MLS data after the threshold cut.

As shown in Figure 4.1 (a), the raw MLS data have large proportion of redundant data. Figure 4.1 (b) shows that the buildings and other objects far from the trajectory can be removed after the threshold cut. However, during the process, some of the trees cut into separated parts, as shown in the left side of Figure 4.1 (b) and may be neglected during the clustering process.

4.1.2 Outlier Removal

As can be seen from Figure 4.2 (a), some outlier points are in the air and some have a lower elevation than the ground surface, which can cause trouble for ground removal algorithms. Two parameters need to be set in this method: the number of nearest points used

in the mean distance estimation process and the SD multiplier threshold. To remove some clustered outliers and keep the tree points, different thresholds need to be tested. Finally, the number of nearest points was set as 30 and the SD multiplier was set as 5. The processing speed of the algorithm was about 30 seconds for a 100MB scene based on the selected parameters. Figure 4.2 (b) shows the data after the outlier points are removed. However, the method cannot remove outliers that are clustered and near the object surface.

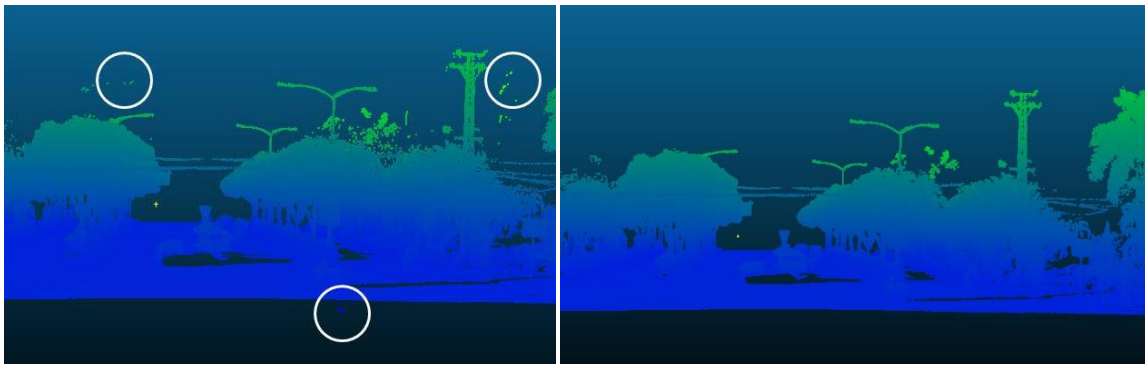

(a) (b)

Figure 4.2: Outlier removal results. (a) Outliers found in raw MLS data. (b) MLS data after outlier removal.

4.1.3 Ground Removal

Four parameters were needed for the upward growing ground removal method: the local terrain relief was set as 0.3 m, the global terrain relief was set around 5m, and the voxel resolution was set as 5 cm. As can be seen in Figure 4.3, the method can remove most of the ground points from the datasets. The processing speed of the algorithm was about 5 seconds for a 100MB scene based on the selected parameters.

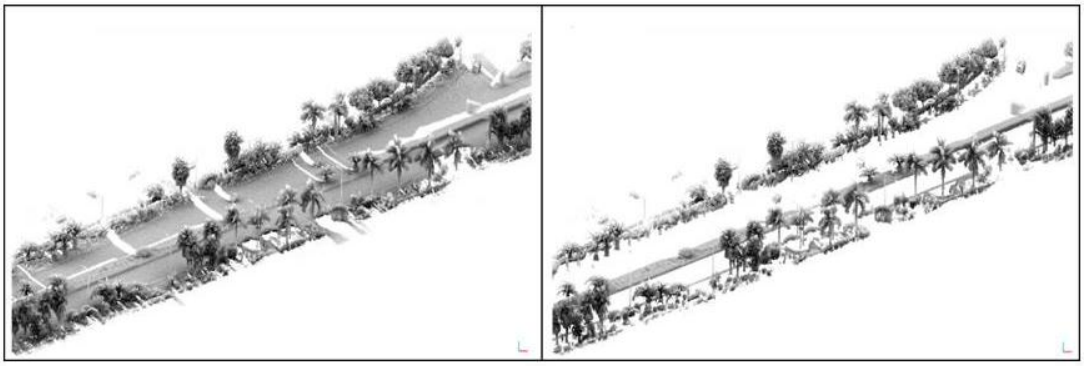

(a) (b)

Figure 4.3: Ground removal results. (a) MLS data before ground removal. (b) MLS data after ground removal.

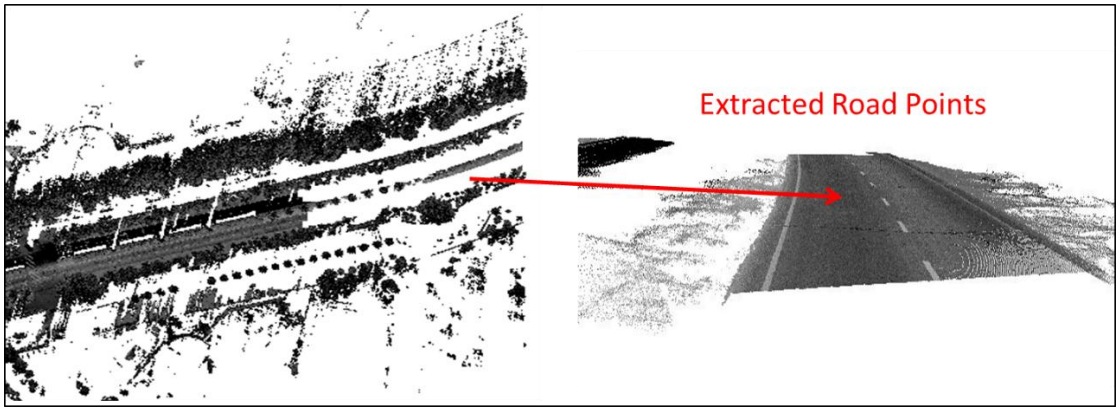

Figure 4.4: Ground points removal using 2m global relief.

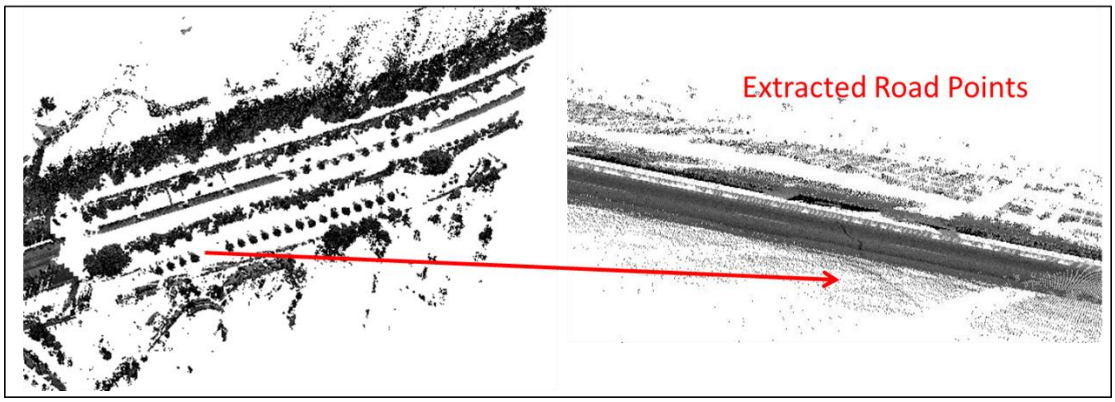

Figure 4.5: Ground points removal using 10m global relief.

However, the global relief set by the user may affect the filtering results. For example, Figure 4.4 shows that the higher road points were not extracted when using a 2 m global relief threshold. This can be solved by dividing the road into smaller scenes. This problem can also be solved by changing the global relief threshold to a larger value. Figure 4.5 shows the result when the global relief was set as 10 m. However, this can lower the time efficiency of the algorithm by around 10 seconds, and some of the points and small clusters were filtered as ground points as shown in the right side of Figure 4.5. These error points may affect the generation of DTM. However, their impact on tree species classification and tree extraction is smaller.

4.1.4 Clustering

(1) Euclidean Clustering

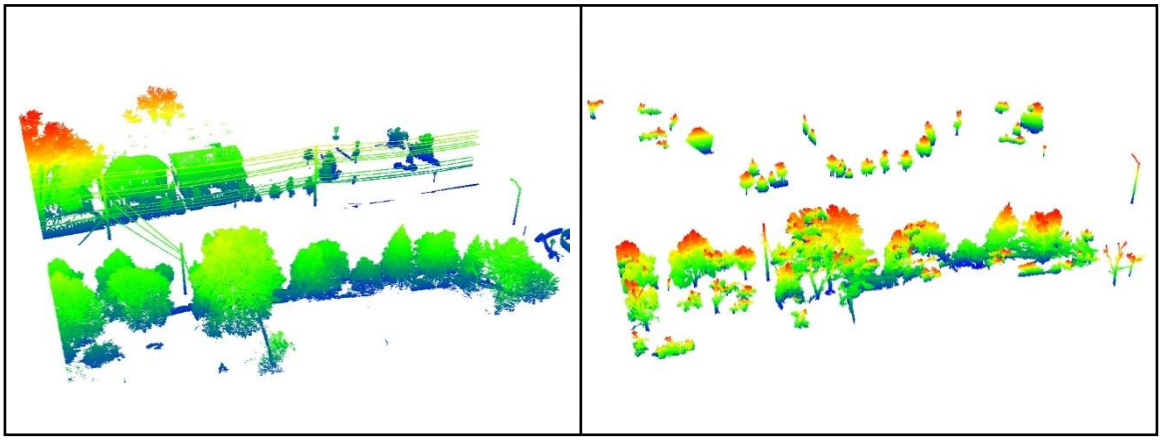

(a) (b)

Figure 4.6: Clustering result of Euclidean distance method using Dataset D. (a) MLS data before clustering. (b) MLS data after clustering.

As can be seen in Figure 4.6 (a), the point density of tree crowns are very small when far from the trajectory. Thus, the bigger tree crowns were often segmented into two parts based

on the distance threshold. As can be seen in Figure 4.6 (b), trunks are only segmented for some of the trees far from the trajectory. Also, some trees connected to houses were not successfully segmented.

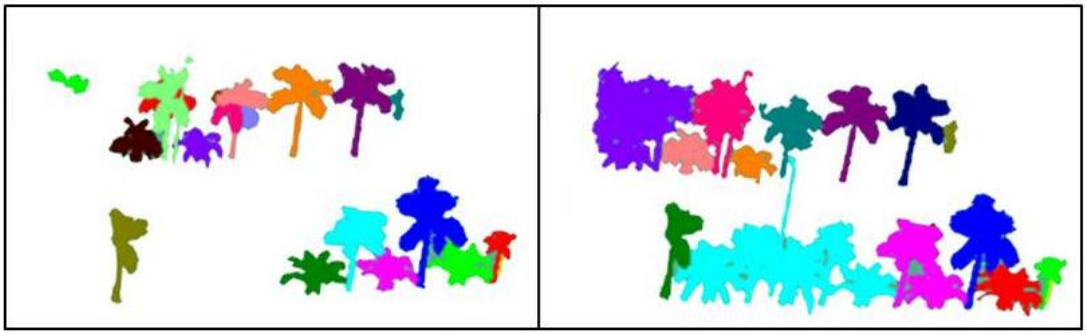

(a) (b)

Figure 4.7: Clustering results of the Euclidean distance method. (a) Clustering result using a smaller distance threshold. (b) Clustering result using a larger distance threshold.

However, for Datasets A, B, and C, which have a lower point density and smaller tree crowns, the method can achieve acceptable segmentation results. Figure 4.6 shows the clustering results when different parameters were applied. The distance threshold was set as 0.1 m and 0.3 m in Figures 4.7(a) and 4.7 (b); the number of neighbor points was set as 30 in both tests; the cluster size threshold was set as 500 points minimum. The result shows that a large threshold will merge connected trees. Although these connected trees can be separated using a smaller threshold, some trees can be clustered into small parts.

(2) Region Growing Segmentation

Parameters for region growing segmentation can affect the segmentation result and need to be tested for different datasets. Although the method can segment some of the connected trees by setting a smaller searching neighbor number or smaller thresholds, the tree trunks were often segmented apart from tree crowns. However, the method can be used to extract tree trunks by setting a smaller smoothness threshold. Generally, the region growing segmentation can produce better segmentation results than the Euclidean clustering method. However, the processing speed of the method is much slower than the Euclidean clustering method.

Table 4.1: Parameters for Region Growing Segmentation.

	Number of neighbours	Smoothness threshold	Curvature threshold	Normal estimator number of neighbours	Minimum points
Figure 4.8(a)	15	1/6	0.4	15	1000
Figure 4.8(b)	30	1/6	0.4	30	1000
Figure 4.9(a)	15	1/6	0.1	15	2000
Figure 4.9(b)	15	1/18	0.4	15	1000

Table 4.1 shows the parameters used in the region growing method. It can be seen by comparing Figure 4.8 (a) and 4.8(b) that some of the tree trunks were separated from the tree crowns when the search number of their neighbours was set as 15. Figure 4.9(a) and 4.9 (b)

show that setting a smaller smoothness threshold is better for extracting tree trunks. However, small trees were not detected using this method.

(a) (b)

Figure 4.8: Segmentation results of the region growing method.

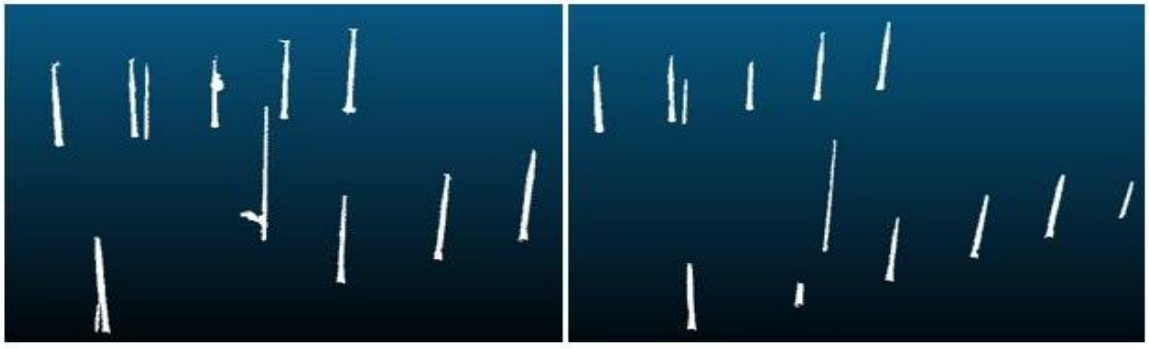

(a) (b)

Figure 4.9: Tree trunk extraction results of the region growing method.

(3) Ncut

The MLS data has high point densities that require too much memory space when processed using the Ncut method. Thus, the original dataset, as shown in Figure 4.10 (a), was subsampled to the cloud shown in Figure 4.10 (b). The point number decreased from 36901 to 5367 to enable the data to be processed using the Ncut method. As can be seen from Figure 4.10 (c), the segmentation can separate electricity poles from the trees. Figure 4.10 (d)

shows that the method can also segment connected trees. However, the method requires a manually defined number of clusters and may not work for big clusters.

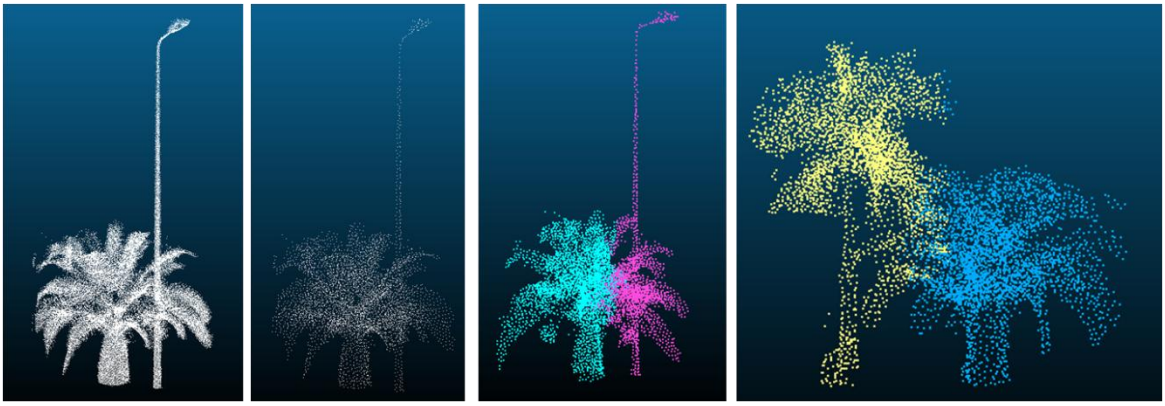

Figure 4.10: Segmentation results of the Ncut method. (a) A cluster that was not successfully segmented using the Euclidean distance clustering method. (b) Downscaled high density point cloud. (c) The segmentation result when the method was used to segment connected trees and light poles. (d) The segmentation result when the method was used to segment connected trees.

Although the clusters with more than one tree can easily be classified and be segmented using the Ncut method, the loss of tree points may cause errors in the geometrical measurement of the tree. Thus, these clusters in Dataset A were discarded. However, the Ncut method can be applied using computers with larger memory space without subsample of point clouds.

(4) Supervoxel-based Segmentation

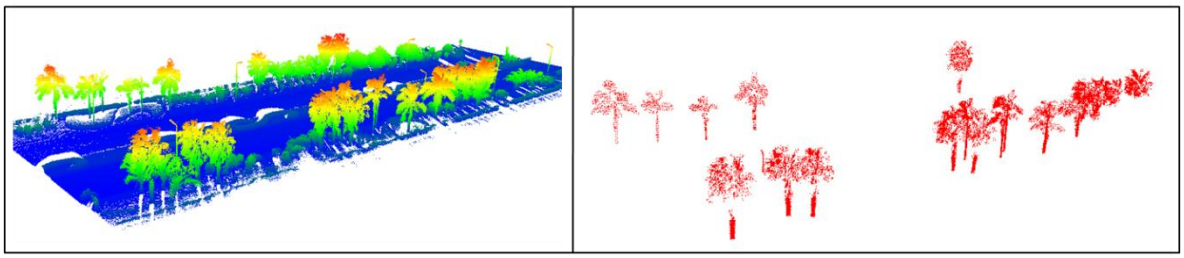

(a) (b)

Figure 4.11: Segmentation results of Dataset C using the supervoxel-based method.

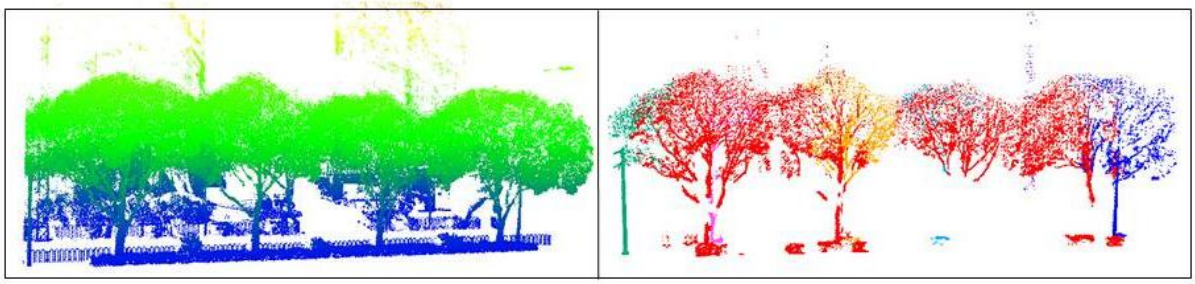

(a) (b)

Figure 4.12: Segmentation results of Dataset B using the supervoxel-based method.

Figure 4.11 shows the tree extraction and segmentation result of Dataset C using the supervoxel based method. The method accurately located the positions of higher trees. However, some smaller trees and trees that were clustered as shown in Figure 4.11 (a) were not detected. Also, around 30% of missing points were found after the segmentation which may lower the point density of the derived clusters. Compared with Datasets A and C, the correctness and completeness of the method was lower when applied to Dataset B as shown in Figure 4.12. Firstly, the problem of over segmentation was indicated by different clours in

Figure 4.12 (b). Secondly, the tilt and brunching of trunks in Dataset B may have caused the errors in the region growing algorithm.

One of the advantages of the supervoxel-based method is that it can segment trees that were connected to electrical poles and road signs. However, as shown in Figure 4.13, the result may not be as accurate as that of the Ncut method.

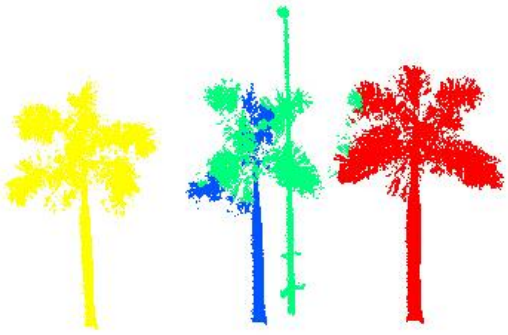

Figure 4.13: Segmentation results of connected trees and electricity poles using the supervoxel-based method.

(5) Errors in the Segmentation Process

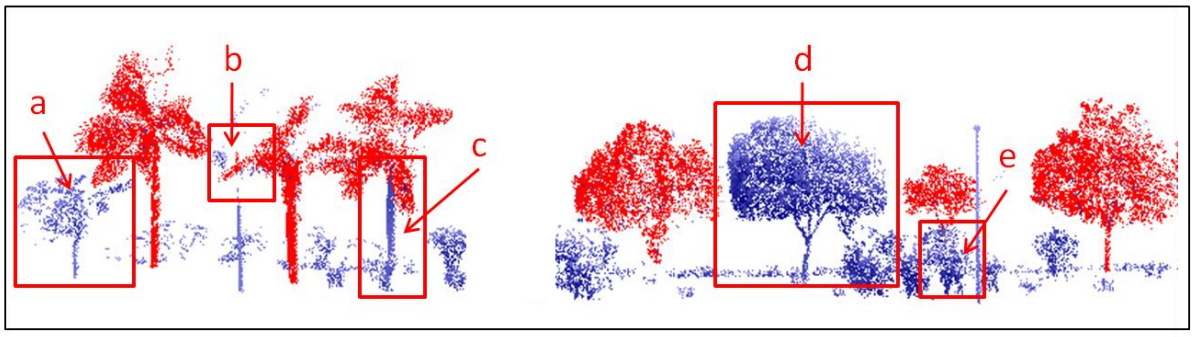

Figure 4.14: Errors and undetected trees.

Figure 4.14 shows some types of errors in the segmentation results (detected trees are shown in red): (a) small trees that were excluded due to smaller point number in the clusters, (b) errors caused by electrical poles or road signs, (c) unconnected tree parts, (d) errors caused by closely connected trees and bushes, (e) occlusion problems caused by bushes .

The results of the Euclidean distance segmentation were adopted for the following methods. The undetected tree rates of the method for Datasets A B and C were 4.7%, 10.7%, and 2.7%. Dataset B obtained the lowest detection rate because the trees in part of Dataset B were planted in two rows, which caused occlusion problems. The segmentation result was more accurate for Dataset C, which may indicate that segmentation of trees with similar sizes and species is easier than segmentation of trees with different sizes and species.

4.2 Estimation of Tree Parameters

4.2.1 Tree Trunk

(1) Trunk Slices Extraction

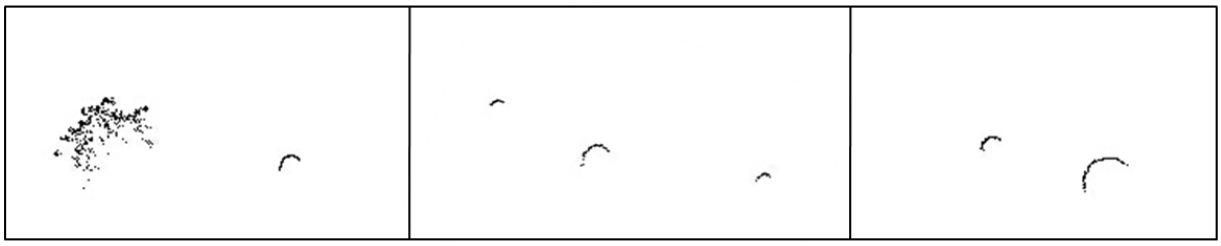

(a) (b) (c)

Figure 4.15: Extracted tree trunk slices.

Figure 4.15 shows the results for tree trunk slices extraction. After the tree clusters were extracted using segmentation and clustering methods, a pass through filter was used to extract trunk slices. The height of the trunk slices were set at 20cm to ensure enough points for the cylinder fit algorithms. However, since the segmentation results are not perfect, some of the bushes, as shown in Figure 4.15(a), electrical poles, as shown in Figure 4.15(b), and tree leaves, as shown in Figure 4.15(c) were also cut into the slices. Although most of the bushes and electricity poles can be removed by setting the distance threshold and cluster width during the clustering of trunk slices, some of the smaller clusters that are not sparsely distributed can be misclassified as tree trunks.

(2) Cylinder Fit

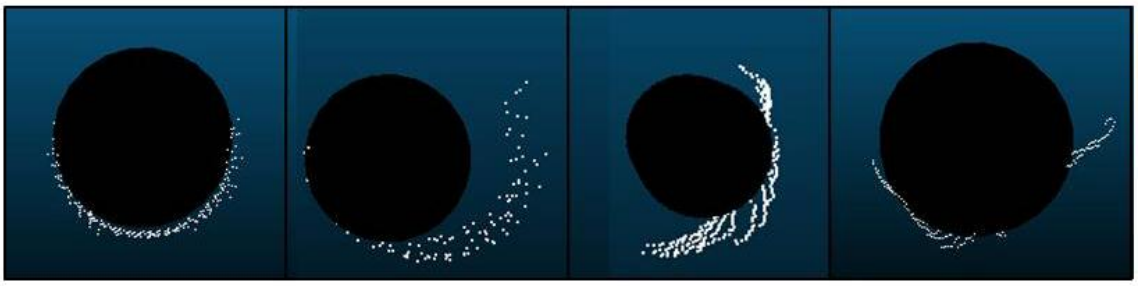

(a) (b) (c) (d)

Figure 4.16Cylinder fit results and problems

Although the cylinder fit method can accurately represent most of the tree trunks, as shown in Figure 4.16 (a), it can create certain errors in three cases. Firstly, some of the tropical vegetation has very coarse trunks as shown in Figure 4.16 (b). Secondly, some of the trees have bumps on the trunk as shown in Figure 4.16 (c). Lastly, some of the trees have an

irregular trunk shape, as shown in Figure 4.16 (d). Among 128 trees selected in Dataset B, 21.1 % of the tree trunk diameters had estimated errors larger than 20 cm. Since the cylinder method cannot produce a stable result of DBH estimation using trunk slices, another Minimum Bounding rectangle method was applied.

(2) Minimum Bounding Rectangle

The minimum bounding Rectangle method can produce a more stable result than the cylinder fit method. Figure 4.17 shows the predicted tree trunk centers for each trunk horizontal slice. As can be seen from Figure 4.17(a), the method can also estimate tree trunks with low point density. Moreover, the method can estimate DBH for irregular trunk shapes as shown in Figures 4.17(b) to 4.17(d). However, the method tends to underestimate the DBH.

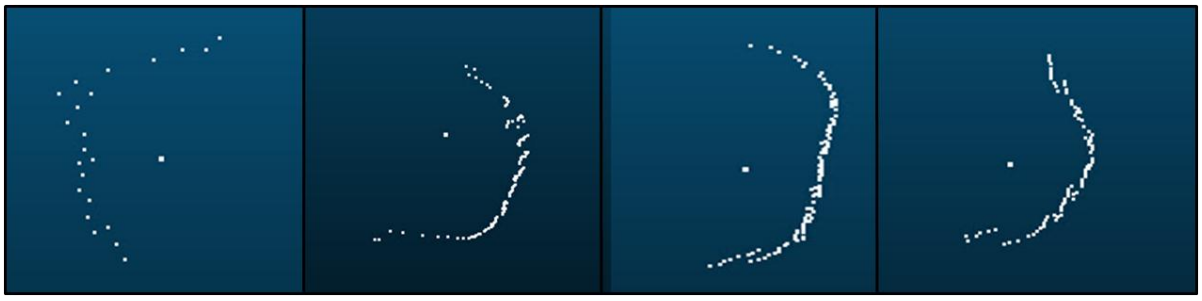

(a) (b) (c) (d)

Figure 4.17 Results of obtained tree centers using the minimum bounding rectangle method.

4.2.2 Tree Crown

(1) 2D Alpha Shape Outline Extraction

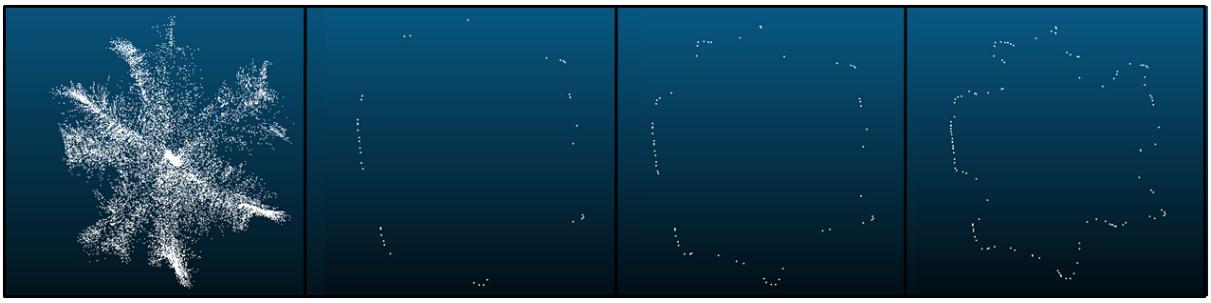

(a) (b) (c) (d)

Figure 4.18: Extracted crown outlines using the 2D alpha shape method.

The result of crown outline extraction can be affected by the radius of the alpha shape. Figure 4.18 (a) shows the tree crown for a coconut tree in Dataset B. The radius was set as 5, 1, and 0.1 in Figure 4.18 (b), (c), and (d), respectively. Although the method can produce a more detailed outline by setting a smaller radius, the computation speed may be lowered.

(2) Segmentation of Crown Outline

Figure 4.19(a) shows the segmentation of the crown outline using tree trunk locations and estimated crown radius; Figure 4.19 (b) shows the original point cloud. As can be seen from the figure, the edge of each dataset can cause errors in the segmentation. Also, this method relies on the location of tree trunks. Thus, missing or misclassified tree trunks can cause errors in the segmentation results.

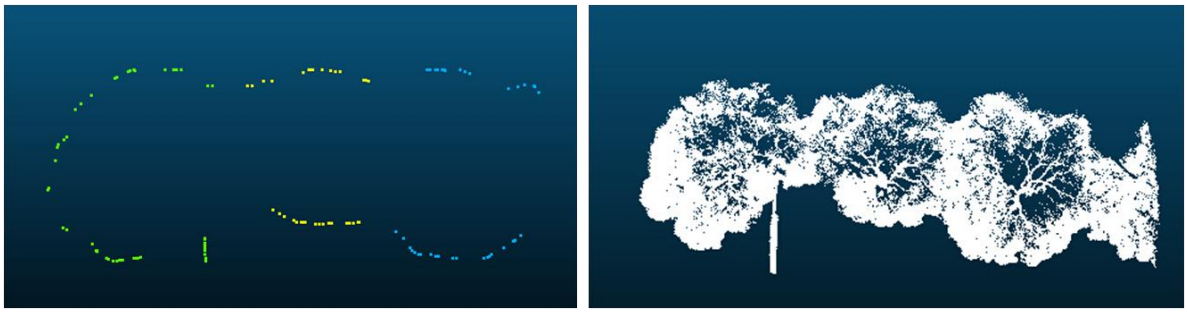

(a) (b)

Figure 4.19: Results of single tree crown extraction.

(3) Crown Diameter Estimation

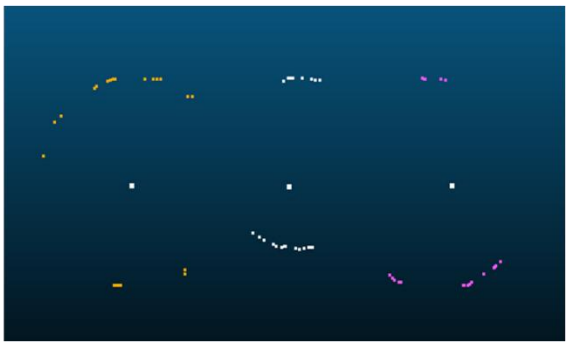

Figure 4.20: Single tree crown extraction.

Figure 4.20 shows the points that were selected to fit the circular model using RANSAC shape detection method. As can be seen in the figure, the method can accurately represent tree crowns for trees with a sphere crown shape.

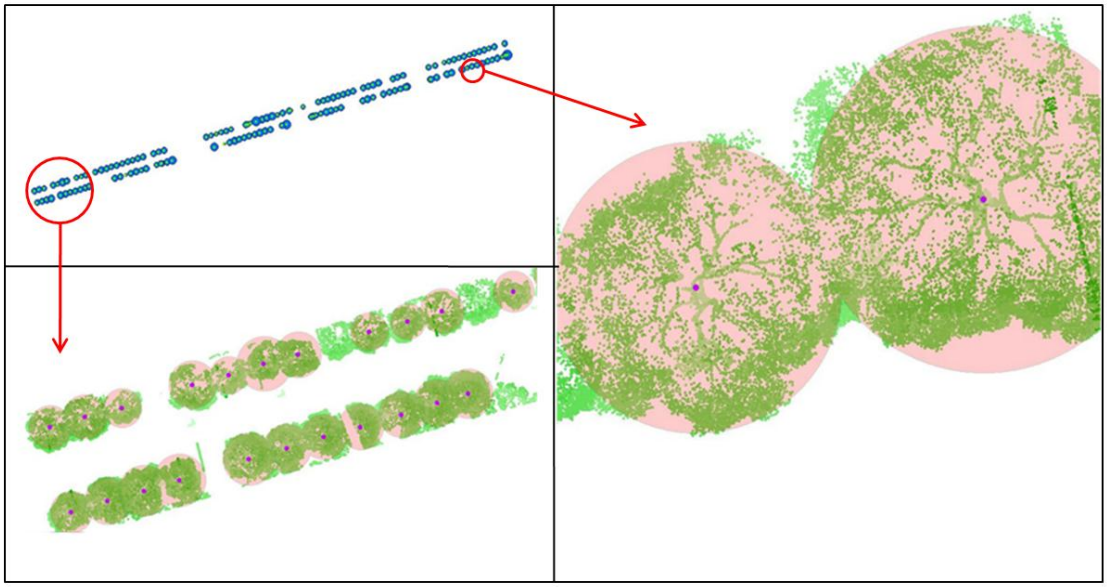

Figure 4.21: Results of crown diameter estimation.

Figure 4.21 shows the result of the crown diameter estimation of Dataset B overlaid with the original point clouds. As can be seen from the figure, the proposed method can estimate crown diameter when trees are connected and deal with missing data. Also, the tree trunks were successfully located within true trunk boundaries using the center of the minimum bounding boxes. However, the electrical poles and road signs caused errors in estimation.

4.2.3 Tree height, SD and Horizontal Slice Features

Table 4.2: Feature Characteristics of Derived Tree Clusters.

t	Average	SD	Maximum	Minimum
Height (m)	8.27	2.36	14.03	2.55
Total point number	13912.09	15589.79	164857.00	1026
Density 0-25% (Points/m^2)	839.53	4744.70	62216.47	0
Density 40-55% (Points/m^2)	514.10	2699.09	41153.30	0
Density 55-70% (Points/m^2)	269.15	482.66	7082.54	0
Density 95-100% (Points/m^2)	408.29	1633.68	20755.76	0
Point percentage 0-25%	0.10	0.07	0.54	0.02
Point percentage 40-55%	0.19	0.08	0.46	0.03
Point percentage 55-70%	0.27	0.09	0.49	0.02
Point percentage 95-100%	0.02	0.03	0.20	0

After tree clusters were extracted, various features were derived: height, cluster width, total point number, SD of point heights, point density in different horizontal slices, and point number percentile in different horizontal slices. Table 4.2 shows the characteristics of some of the derived features. The SD of the total point number in clusters is very large because some of the clusters have more than one tree and some trees may be connected to bushes. As can be seen from the table, some of the clusters' minimum point density and minimum point percentage are 0. This can be caused by fewer points on the tree top or very small clusters. The minimum point number is 1026 because clusters that have a smaller size were excluded during the segmentation process.

4.3 Classification

Since some of the trees were not segmented into single tree clusters, these clusters were classified into single tree clusters and other clusters using RF classifier. All features

were used during the classification. Table 4.3 shows the classification result of the method; the overall accuracy of the method was 94.6%. The clusters that contain more than one tree can be re-segmented using the Ncut method or the supervoxel-based segmentation method.

Table 4.3: Classification Result of Derived Clusters

		Predicted		
		Other clusters	Single tree clusters	Error
Observed	Other clusters	62	13	0.17
	Single tree clusters	2	202	0.01

4.3.1 Feature Selection

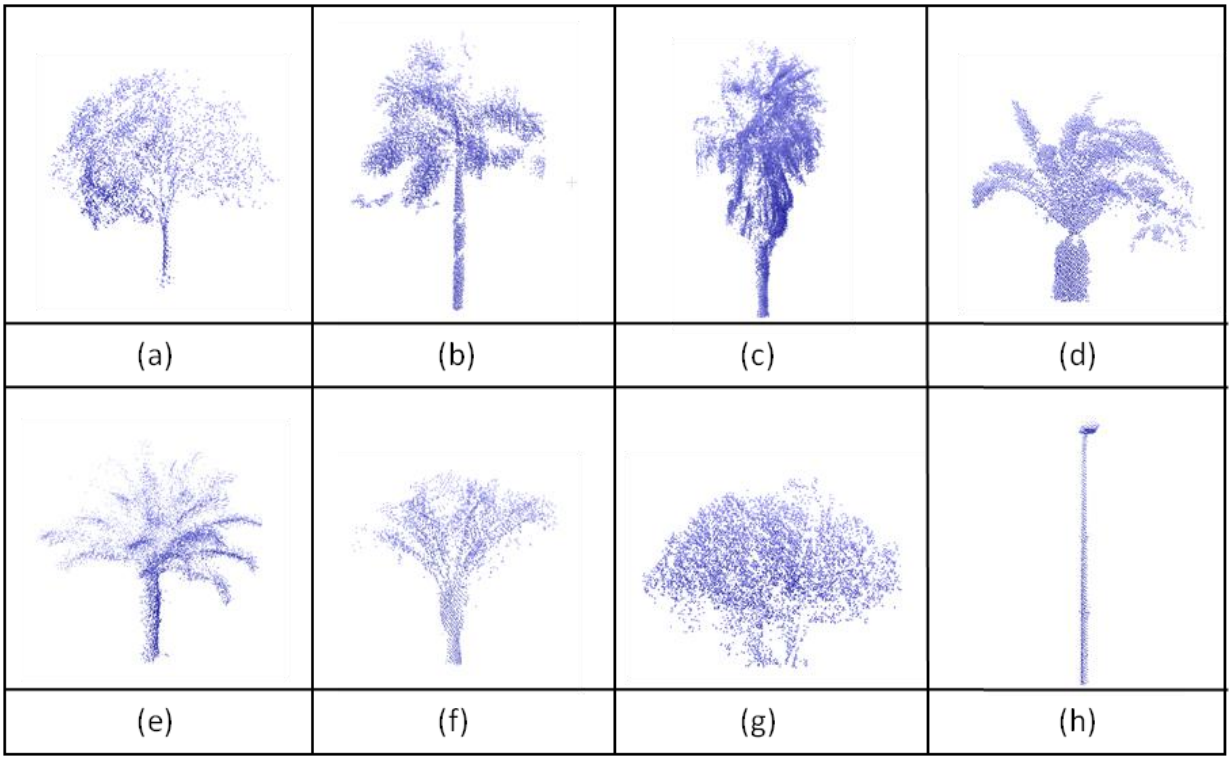

Figure 4.22: Different tree species and a light pole in Dataset C.

After single tree clusters were separated from other clusters, the single tree clusters were manually labeled as different classes. The names of the tree clusters and light poles shown in Figure 4.22 are *Bischofia polycarpa*, *Roystonea regia*, *Washingtonia filifera*, *Sago cycas*, *Sylvester palm*, *Triangle palm*, bush, and light pole from (a) to (h).

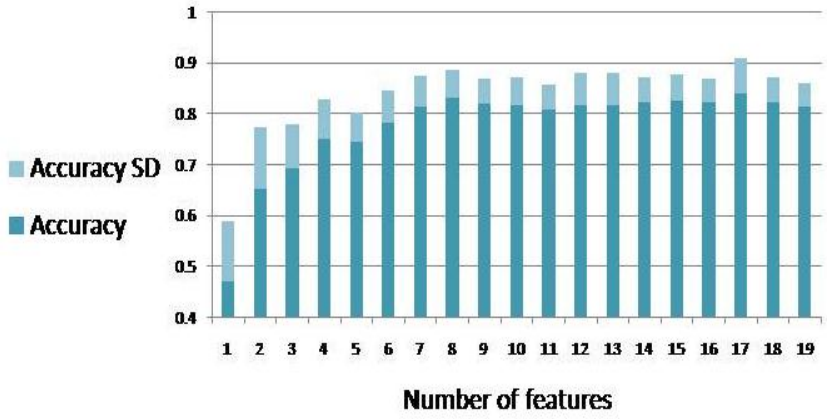

Figure 4.23: Accuracy and standard deviation for a different number of variables.

Figure 4.23 shows the accuracy and SD of accuracy of classification using different input sizes. For the purpose of reducing the input feature number, achieving high accuracy, and low SD of accuracy, the number of input features was set as 14.

Table 4.4 shows the features' importance for 8 different tree types of cluster. Finally, top 14 features with high importance were extracted: Height, x-width, y-width, SD, Density 40-55 %, Density 55-70 %, Density 70-85 %, Density 85-95 %, Density 95-100 %, Point number 0-25 %, Point number 25-40 %, Point number 40-55 %, Point number 85-95 %, and Point number 95-100 %.

Table 4.4: Importance of Different Variables for Different Class Types

	BP	RR	WF	SC	SP	TP	B	LP
Height	0.9939	0.9354	0.9987	1	1	1	0.8907	1
x-width	1	1	1	1	1	1	1	1
Y-width	1	1	0.9981	1	1	1	1	1
SD	0.9855	1	0.9952	1	1	1	0.96	1
Total point number	0.9987	0.9804	0.9808	1	0.9455	0.96	0.94	1
Density 0-25%	0.8782	0.8782	0.8654	0.6587	0.7	0.82	0.9	0.9
Density 25-40%	0.8453	0.9	0.6566	0.8375	0.7591	0.9	1	0.8
Density 40-55%	0.9	0.9208	0.8394	0.9875	0.9	0.98	1	0.9
Density 55-70%	1	0.9667	0.9952	1	1	1	1	1
Density 70-85%	0.894	0.9	0.9981	0.95	0.9	0.92	0.9981	0.901
Density 85-95%	0.9667	0.9667	1	1	0.9773	1	0.9769	1
Density 95-100%	0.7693	0.86	0.7587	0.95	0.6955	0.9	0.95	0.6781
Point number 0-25%	0.896	0.9267	1	1	0.9818	1	0.92	1
Point number 25-40%	0.9067	0.8	0.9385	0.9375	0.8409	0.9	1	0.95
Point number 40-55%	0.9013	0.6867	0.8904	0.9375	0.8727	1	1	1
Point number 55-70%	0.9533	0.9067	0.9471	1	1	1	0.94	1
Point number 70-85%	0.9133	0.9133	0.9077	0.9187	0.8727	0.95	1	0.9133
Point number 85-95%	0.9008	0.8867	0.8517	0.9125	0.7545	0.8812	0.9125	0.9125
Point number 95-100%	1	1	1	1	1	1	1	1

4.3.2 Classification

(1) K-Nearest Neighbour

Firstly, the value of k was tested and selected. As can be seen in Figure 4.23, when the k value equals 2, 3 and 4, the method achieved the highest accuracy, so the k value was selected as 3.

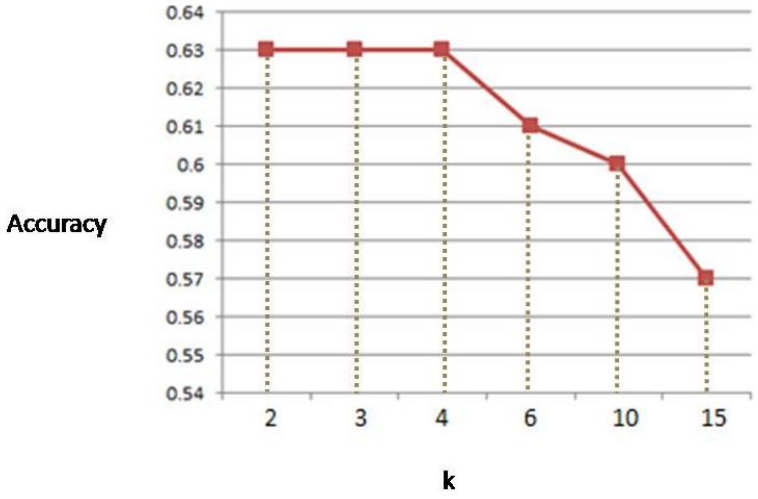

Figure 4.24: Accuracy for different k values.

Table 4.5: Confusion Matrix of k-Nearest Neighbour Classification.

	BP	RR	WF	SC	SP	TP	B	LP	Total	Completeness
BP	8	5	0	0	1	0	1	0	15	0.53
RR	0	56	31	13	1	3	0	0	104	0.54
WF	0	2	30	0	0	0	0	0	32	0.94
SC	1	0	0	15	2	4	0	0	22	0.68
SP	3	0	0	2	4	1	0	0	10	0.40
TP	0	0	0	0	0	6	0	0	6	1
B	2	0	0	1	0	1	2	0	6	0.33
LP	0	1	0	0	0	0	0	9	10	0.90
Total	14	64	61	31	8	15	3	9	205	
Correctness	0.57	0.88	0.49	0.48	0.50	0.40	0.67	1	Overall accuracy=0.630	

Table 4.5 shows the confusion matrix of classification using the k-NN method. The result shows that (1) around 30% of RR were classified as WF because the two tree species share similar geometrical shapes, (2) the light poles can be easily separated from trees, (3) smaller trees such as BP, SP, TP and B are more difficult to classify.

(2) Random Forest

As can be seen from Table 4.6, the overall accuracy of classification using the RF method is much higher than the k-NN method. However, the classification of similar tree species is still a problem. Some of the classes have lower classification accuracy than the other classes such as BP, SP, TP and B. This can be caused by insufficient training samples in the selected area.

Table 4.6: Confusion Matrix of Random Forest Classification

	BP	RR	WF	SC	SP	TP	B	LP	Total	Completeness
BP	8	5	0	0	1	0	1	0	15	0.53
RR	0	83	17	1	1	2	0	0	104	0.80
WF	1	2	28	1	0	0	0	0	32	0.88
SC	0	2	0	17	0	3	0	0	22	0.77
SP	0	1	0	1	4	2	2	0	10	0.40
TP	0	0	0	0	0	6	0	0	6	1
B	0	0	0	0	0	2	4	0	6	0.67
LP	0	0	0	0	0	0	0	10	10	1
Total	9	93	45	20	6	15	7	10	205	
Correctness	0.89	0.89	0.62	0.85	0.67	0.4	0.57	1	Overall accuracy =0.781	

4.3.3 DBH Estimation

(1) DBH Estimation Result using the Bounding Rectangle Method

Table 4.7 shows the result of the DBH estimation for different datasets. Due to the occlusion problem in some of the datasets, 151 of 163 trees surveyed were included in the accuracy assessment. It can be seen from Table 4.7 that the minimum bounding rectangle method tends to underestimate the DBH because the MLS data used in this study cannot

capture more than half of the tree trunks all the time. Dataset A received the lowest overall accuracy in the tree datasets because the data is noisier than the other two datasets. The overall accuracy of Dataset C is lower than Dataset B because the tree trunks in Dataset C are not as symmetrical as trunks in Dataset B. Also, the field survey data for Dataset C may be less accurate than that of Dataset B for three reasons: (1) some of the trees in Dataset C have rough bark which may cause inaccurate perimeter measurements, (2) the ground in Dataset C is uneven and has very soft soil on the surface, which may cause inaccurate height measurements, (3) some of the trees in Dataset C start to branch at 1m height which leads to enormous DBH changes around the trunk slice in the area.

Table 4.7: Overall Accuracy and RMSE for DBH Estimation Using Minimum Bounding Rectangle Method

Dataset	Average DBH Estimated (cm)	Average DBH Reference (cm)	Overall Accuracy	RMSE (cm)
A	29.0	32.1	0.902	6.6
B	33.1	33.9	0.975	4.9
C	41.2	44.5	0.926	7.3
All	34.8	36.8	0.946	5.0

(2) Linear Regression of DBH Estimation

Firstly, the regression accuracy was enhanced by removal of outlier inputs. Figure 4.25 shows the ten outliers that were removed from the regression model.

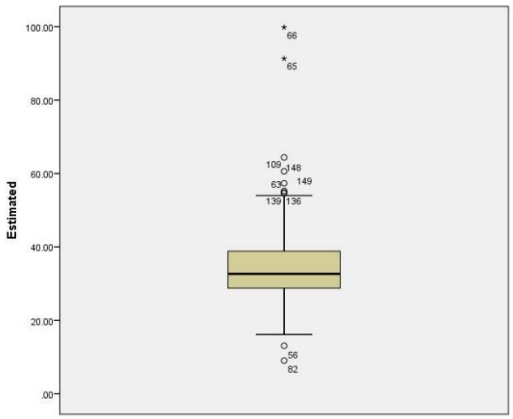

Figure 4.25: Outlier removal of linear regression inputs.

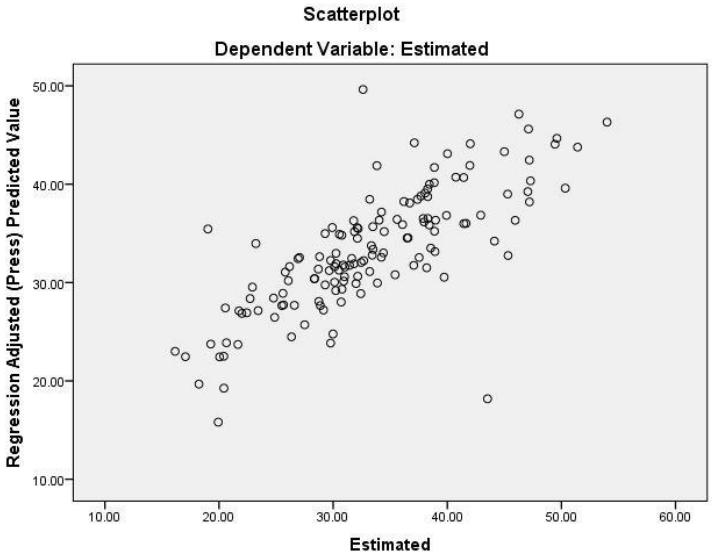

Figure 4.26: Linear regression of DBH using all data inputs (cm).

Figure 4.26 shows the linear regression result of DBH estimation using the remaining 141 inputs. The R^2 of the estimation is 0.602; the standard error of the estimation is 5.0 cm. The linear regression parameters are shown in the following equation:

$$D=0.734d+6.788 \quad (4.1)$$

Where d is the derived DBH, D is the regression adjusted DBH.

Table 4.8: Regression Results of Different Datasets Using Bounding Rectangle Method And Cylinder Fit Method.

Dataset	Method	R^2	Standard error (cm)
A	Bounding Rectangle	0.422	3.9
B		0.426	5.7
C		0.765	4.0
A	Cylinder fit	0.025	8.8

Table 4.8 shows the R^2 and standard error of estimation for the three datasets and the result of the cylinder fit for Dataset A. For 53 trees in Dataset A, 9 of the trunk slices failed to fit the RANSAC cylinder detection method. Ten of the 44 derived DBH results had a higher error than 2 times RMSE. As can be seen from Table 4.8, the R^2 of the cylinder fit method is also very small and the standard error is much higher than that of the bounding rectangle method.

Dataset C achieved the highest R^2 among the three datasets; however, the standard error of Dataset C is nearly the same as Dataset A. As can be seen in Figure 4.27 (c), the trees in Dataset C have a larger range of DBH due to the variety of tree species. Dataset A received the lowest R^2 and the points are more scattered as shown in Figure 4.27 (a), because of small trees that were planted near big trees and heavy occlusions in the dataset.

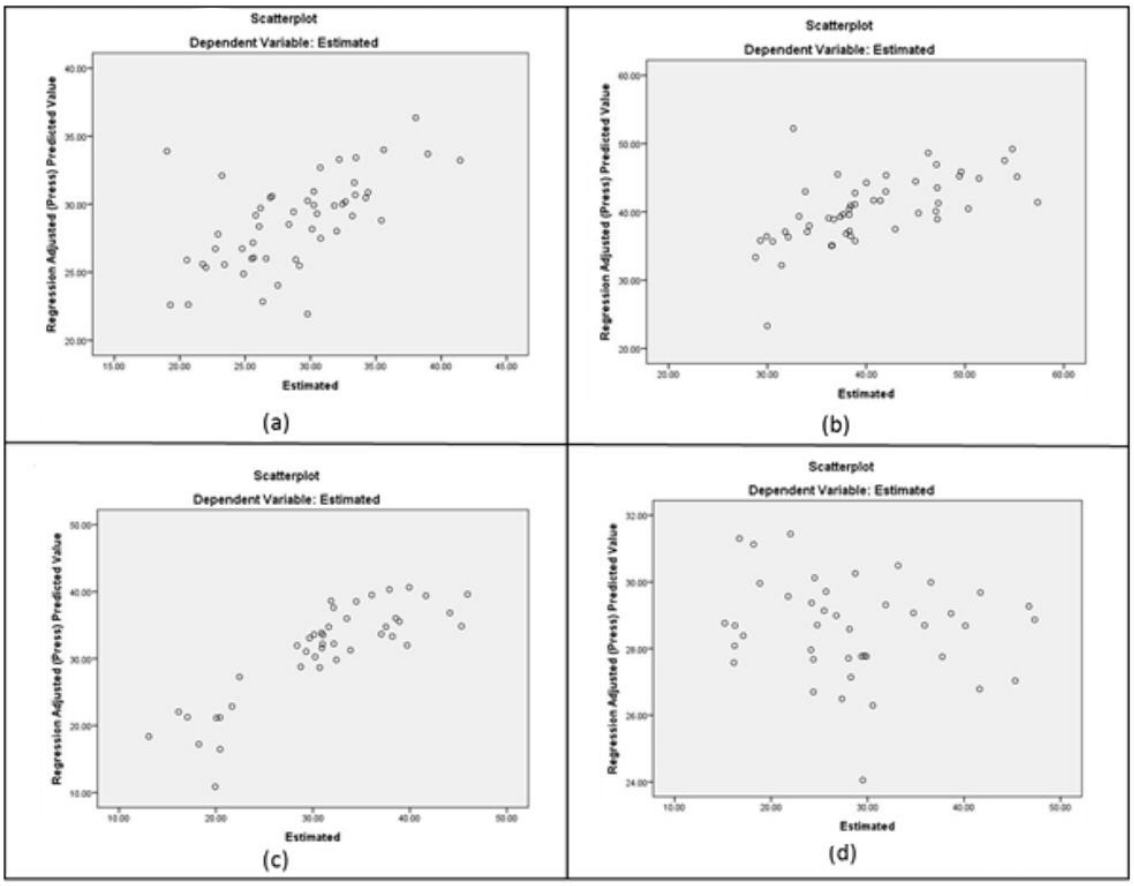

Figure 4.27: Linear regression of DBH estimation. (a)Result of Dataset A using the bounding rectangle method. (b) Result of Dataset B using the bounding rectangle method. (c) Result of Dataset C using the bounding rectangle method. (d) Result of Dataset A using the RANSAC cylinder fit method.

4.4 Chapter Summary

This chapter has presented the results of the extraction of single trees, parameter estimation, and classification. In the section on extraction of single trees, firstly, the importance of outlier point removal was discussed. Secondly, the advantages and problems of the voxel-based upward growing ground filtering method were discussed. Thirdly, results

of three segmentation methods (the Euclidean distance clustering, the region growing segmentation, and Ncut) were compared. In the parameter estimation part, the results of derived geometrical measurements were presented. In the classification part, the classification results of two methods, k-NN and RF, were presented using a confusion matrix. Lastly, the accuracy assessment of DBH estimation using field survey data and linear regression was discussed.

Chapter 5
Conclusions and Recommendations

This chapter presents the conclusions of this study, summarizes the experiences, pinpoints the limitations and gives suggestions for future studies.

5.1 Conclusions

The results of this study show that MLS can be helpful for urban roadside tree inventory and achieves higher time-efficiency, and better species classification and DBH estimation results than ALS.

Since raw MLS data is often very large and objects far from the trajectory cannot be well captured, points far from the trajectory are often removed from the dataset. Also, the dataset must be divided into smaller files to be processed. The result of such processes may lead to objects near the separation line being divided into parts, which may cause errors in later processes.

The removal of outlier points in MLS data can be crucial for ground filters. However, setting a smaller threshold may result in tree points classified as outliers. Also, clustered outliers can be difficult to remove using the statistical outlier removal method.

Ground point removal can enhance segmentation accuracy and efficiency. However, the removal of the ground point can be difficult for MLS data due to the large data volume. The voxel-based upward growing algorithm can remove the ground points with high

accuracy and efficiency. However, the method may have problems when inputting a large dataset with high slope.

There were four segmentation methods compared in this study: the Euclidean distance clustering, the region growing segmentation, the Ncut segmentation, and super voxel based segmentation. The Euclidean distance clustering is simple to use but cannot correctly separate closely connected trees. The Ncut method obtains the best segmentation result and separates closely connected trees. However, the method needs users to observe the number of clusters that need to be segmented and requires too much memory space. The super voxel based segmentation can segment connected trees but it may cause missing points during the process. To obtain better segmentation results and better efficiency, the Ncut method can be applied after the Euclidean distance clustering.

The overall accuracy of tree species classification is around 78 %, which is better than using ALS, but lower than the deep learning method presented in Guan et al.'s study (2015), which was 80%. The waveform transform of horizontal slices' attribute in their study seems better at representing the shape of trees. The classification accuracy increased after using a RFE feature selection method because of the large number of feature types and the noise in the input data. Also, the RF classifier achieved better classification accuracy than k-NN.

Although the RANSAC cylinder fit method can be more accurate than the bounding rectangle method, it is unstable and may not work for irregular tree trunks. However, the bounding rectangle method may not well represent the tree trunk center when not enough tree

trunk points are processed. The circle fit method can be used to represent round crowns, but the 2D alpha shape method can be used to estimate tree crowns with different shapes. The overall accuracy of DBH estimation using the bounding rectangle method is around 95 %, which is slightly better than statistical methods for ALS data, which is around 90 %.

5.2 Limitations and Recommendations

(1) Occlusions

To reduce occlusions, the survey should be conducted when fewer people and cars are on the roads. Also, surveying from two directions or two sides of trees can achieve better data for DBH estimation. The occlusions at the bottom of tree trunks may result in error in the height estimation. Thus, future studies may use the trunk position information and ground points' height near the trunk to calculate the tree height. The occlusions at the trunk slices may result in error to the DBH estimation. Thus, future studies may cut more than one horizontal slice to estimate the DBH. If the difference between the slices exceeds a certain value, the tree should be processed separately; if the derived DBH are the same, the trunk can be a misclassified electricity pole. Also, better estimation methods that can work for all kinds of tree trunks are needed to improve the cylinder fit and the bounding rectangle method.

Occlusions can also cause problems for DBH estimation for conifer trees because the tree trunks are often occluded by brunches. The extraction of such trunks can be difficult using only segmentation methods. However, the intensity value may be helpful to separate trunk points from leaf points.

(2) Point Density

The high point density of MLS data can cause 3 problems: (1) the data have to be cut into small pieces which may cut trees into two parts; (2) some parts of tree points may be removed when the threshold cut method is used to remove points that are far from the trajectory; (3) the processing time for the datasets can be very long. For example, the region growing segmentation algorithm takes more than 1 hour to segment a 100 m data using the laptop I mentioned before and the Ncut method takes around 30 minutes to segment two connected trees.

The uneven point density in MLS can also cause problems for segmentation algorithms based on distances between nearest points. Thus, the user defined thresholds may not work for trees far from the trajectory. Also, trees with a wide crown spread can be segmented into two parts due to the point density change. For future studies of high point density MLS data which have large trees in the surveyed area, the normalization or subsampling of the point cloud may be necessary.

(3) Other Limitations

The classification method proposed in this study may be improved by a waveform transform of tree horizontal attributes or by adding other features. The training samples of this study were randomly selected and some of the tree types only have a few samples. Thus, better classification results can be achieved by adding more samples or by improving the quality of the training samples.

The degree of automation of the proposed method can be improved to achieve better time efficiency. For example, the threshold for the Euclidean distance clustering can be set by algorithms that can automatically examine the point density. Also, the Ncut method can be more practical when the number of clusters can be set automatically.

Another limitation of the method is that it discarded small clusters during the segmentation process. Thus, small trees were not detected. Future studies can include classification of small clusters to extract these small trees.

Intensity and number of return information which can be useful for extracting tree trunks and tree species classification were not included in this study. Also, using true color MLS data or multispectral MLS data may improve the classification accuracy. Another recommendation is sorting the exported point clouds using their X or Y coordinates. This method can enhance the efficiency of manually labeling tree species and DBH reference data.

In summary, this study proves that MLS data can be useful for tree species classification and extraction of geometrical information such as tree height, DBH, and crown diameter. The proposed method achieved higher classification and DBH estimation accuracy when compared with ALS. However, the degree of automation and adaptability of the method can be improved to facilitate practical forestry applications.

References

Aijazi, A. K., Checchin, P., Trassoudaine, L. 2013. Segmentation based classification of 3D urban point clouds: A super-voxel based approach with evaluation. Remote Sensing, 5(4), 1624-1650. doi:10.3390/rs5041624

Armson, D., Stringer, P., Ennos, A. R. 2013. The effect of street trees and amenity grass on urban surface water runoff in Manchester, UK. Urban Forestry & Urban Greening, 12(3), 282-286. doi:10.1016/j.ufug.2013.04.001

Barber, D., Mills, J., Smith-Voysey, S. 2008. Geometric validation of a ground-based mobile laser scanning system, ISPRS Journal of Photogrammetry and Remote Sensing, 63, 128-141.

Bardekjian, A., Kenney, A., Rosen, M. 2016. Trends in Canada's urban forests. Tree Canada.http://www.fao.org/docrep/ARTICLE/WFC/XII/0752-B1.HTM. Accessed 10th March, 2016.

Brandtberg, T., Warner, T. A., Landenberger, R. E., McGraw, J. B. 2003. Detection and analysis of individual leaf-off tree crowns in small footprint, high sampling density lidar data from the eastern deciduous forest in NorthAmerica. Remote Sensing of Environment, 853, 290-303. doi:10.1016/S0034-42570300008-7

Chen, D., Zhang, L., Wang, Z., Deng, H. 2013. A mathematical morphology-based multi-level filter of LiDAR data for generating DTMs. Science China Information Sciences, 5610, 1-14. doi:10.1007/s11432-012-4707-3

Dalponte, M., Bruzzone, L., Gianelle, D. 2011. A system for the estimation of single-tree stem diameter and volume using multireturn IDAR data. IEEE Transactions on Geoscience and Remote Sensing, 497, 2479-2487. doi:10.1109/TGRS.2011.2107744

Dinuls, R., Erins, G., Lorencs, A., Mednieks, I., Sinica-Sinavskis, J. 2012. Tree species identification in mixed baltic forest using LiDAR and multispectral data. IEEE Journal of Selected Topics in Applied Earth Observations and Remote Sensing, 52, 594-603. doi:10.1109/JSTARS.2012.2196978

Edelsbrunner, H., MÄucke, E. 1994. Three dimensional alpha shapes. ACM Transactions on Graphics, 131, 43-72. doi:ACM 0730-0301/94/0100-0042

Foley, D., Andries, D., John, H., Steven, F. 1990. Spatial-partitioning representations; Surface detail. Computer Graphics: Principles and Practice. the Systems Programming Series. Addison-Wesley.

Garestier, F., Dubois-Fernandez, P., Champion, I., Le Toan, T. 2011. Pine forest investigation using high resolution P-band pol-InSAR data. Remote Sensing of Environment, 115(11), 2897-2905. doi:10.1016/j.rse.2010.08.028

Guan H, 2013. Automated Extraction of Road Information from Mobile Laser Scanning Data, PhD Thesis, Department of Geography and Environmental Management, University of Waterloo.

Guan, H., Yu, Y., Ji, Z., Li, J., Zhang, Q. 2015. Deep learning-based tree classification using mobile LiDAR data. Remote Sensing Letters, 6(11), 864–873. doi:10.1080/2150704X.2015.1088668

Haala, N., Petera, M., Kremerb, J., Hunterc, G. 2008. Mobile lidar mapping for 3d point cloud collection in urban areas – A performance test. ISPRS Archives, 37, 1119–1124.

Haralick, R. M., Sternberg, S. R., and Zhuang, X.1987. Image analysis using mathematical morphology, IEEE Transactions on Pattern Analysis and Machine Intelligence, PAMI-9, pp. 523–550. doi: 0162-8828/87/0700-0532

Hedge Funds Consistency Index, 2016. R-Squared, http://www.hedgefund-index.com/d_rsquared.asp. Accessed 10th May 2016.

Holmgren, J., Persson, Å. 2004. Identifying species of individual trees using airborne laser scanner. Remote Sensing of Environment, 90, 415-423. doi:10.1016/S0034-42570300140-8

Hudak, A. T., Crookston, N. L., Evans, J. S., Hall, D. E., Falkowski, M. J. 2008. Nearest neighbor imputation of species-level, plot-scale forest structure attributes from LiDAR data. Remote Sensing of Environment, 1125, 2232-2245. doi:10.1016/j.rse.2007.10.009

Ioannou, Y., Taati, B., Harrap, R. 2012. Difference of normals as multi-scale operator in unorganized point clouds. Computer Vision and Pattern Recognition cs.CV, ARxIV:1209.1759. doi: 10.1109/3DIMPVT.2012.12

Islam, M. N., Rahman, K., Bahar, M. M., Habib, M. A., Ando, K., Hattori, N. 2012. Pollution attenuation by roadside greenbelt in and around urban areas. Urban Forestry and Urban Greening, 11(4), 460-464. doi:10.1016/j.ufug.2012.06.004

Kankare, V., Vastaranta, M., Holopainen, M., Räty, M., Yu, X., Hyyppä, J., Viitala, R. 2013. Retrieval of forest aboveground biomass and stem volume with airborne scanning LiDAR. Remote Sensing, 5(5), 2257-2274. doi:10.3390/rs5052257

Kätsch, C., Kunneke, A. 2006. Forest inventory in the digital remote sensing age. The Southern African Forestry Journal, 206(1), 43-49. doi:10.2989/10295920609505243

Kwak, D., Lee, W., Cho, H., Lee, S., Son, Y., Kafatos, M., Kim, S. 2010. Estimating stem volume and biomass of Pinus koraiensis using LiDAR data. Journal of Plant Research, 123(4), 421-432. doi:10.1007/s10265-010-0310-0

Leverett, B., Bertolette, D. 2014. American forests champion trees measuring guidelines handbook. http://www.americanforests.org/wp-content/uploads/2014/12/AF-Tree-Measuring-Guidelines_LR.pdf. Accessed 10 March 2016.

Li, F., Wang, R., Liu, X., Zhang, X. 2005. Urban forest in china: Development patterns, influencing factors and research prospects. International Journal of Sustainable Development and World Ecology, 12(2), 197-204. doi:10.1080/13504500509469630

Li, J., Hu, B., Noland, T. L. 2013. Classification of tree species based on structural features derived from high density LiDAR data. Agricultural and Forest Meteorology, s 171–172,104–114. doi:10.1016/j.agrformet.2012.11.012

Lin, Y., Holopainen, M., Kankare, V., Hyyppä, J. 2014. Validation of mobile laser scanning for understory tree characterization in urban forest. IEEE Journal of Selected Topics in Applied Earth Observations and Remote Sensing, 7(7), 3167-3173. doi:10.1109/JSTARS.2013.2295821

Lin, Y., Herold, M. 2016. Tree species classification based on explicit tree structure feature parameters derived from static terrestrial laser scanning data. Agricultural and Forest Meteorology, 216, 105-114. doi:10.1016/j.agrformet.2015.10.008

Maguya, A. S., Junttila, V., Kauranne, T. 2013. Adaptive algorithm for large scale dtm interpolation from lidar data for forestry applications in steep forested terrain. ISPRS Journal of Photogrammetry and Remote Sensing, 85, 74-83. doi:10.1016/j.isprsjprs.2013.08.005

McDaniel, M., Nishihata, T., Brooks, C. 2012. Terrain classification and identification of tree stems using ground-based lidar. Journal of Field Robotics, 296, 891-910. doi:10.1002/rob.21422

Meng, Q., Cieszewski, C. J., Madden, M., Borders, B. E. 2007. K nearest neighbor method for forest inventory using remote sensing data. GIScience and Remote Sensing, 442, 149-165. doi:10.2747/1548-1603.44.2.149

Morneau, G. 2005. Green streets Canada urban tree inventory project. http://www.duncan.ca/pdf/Green%20Streets%20Final%20Report_11-Reduced.pdf. Accessed 10 March 2016.

Moskal, M., Zheng, G. 2012. Retrieving forest inventory variables with terrestrial laser scanning TLS in urban heterogeneous forest. Remote Sensing, 41, 1-20. doi:10.3390/rs4010001

Othmani, A., Lew Yan Voon, L. F. C., Stolz, C.,Piboule, A. 2013. Single tree species classification from terrestrial laser scanning data for forest inventory. Pattern Recognition Letters, 34(16), 2144-2150. doi:10.1016/j.patrec.2013.08.004

Pal, M. 2005. Random forest classifier for remote sensing classification. International Journal of Remote Sensing, 26(1), 217-222. doi:10.1080/01431160412331269698

Pal, M. 2009. Kernel methods in remote sensing: a review. ISH Journal of Hydraulic Engineering, 15, Issue sup1, 194-215. https://arxiv.org/ftp/arxiv/papers/1101/1101. 2987.pdf

PCL. 2015. PCL documentation. http://pointclouds.org/documentation/tutorials/#filtering-tutorial. Accessed 10 March 2016.

Pingel, T. J., Clarke, K. C., McBride, W. A. 2013. An improved simple morphological filter for the terrain classification of airborne LIDAR data. ISPRS Journal of Photogrammetry and Remote Sensing, 77, 21-30. doi:10.1016/j.isprsjprs.2012.12.002

Pirotti, F., Guarnieri, A., Vettore, A. 2013. Ground filtering and vegetation mapping using multi-return terrestrial laser scanning. ISPRS Journal of Photogrammetry and Remote Sensing, 76, 56-63. doi:10.1016/j.isprsjprs.2012.08.003

Pokorny, J. 2003. Urban tree risk management: A community guide to program design and implementation USDA Forest Service. https://www.na.fs.fed.us/spfo/pubs/uf/utrmm/urban_tree_risk_mgmnt.pdf. Accessed 10 March 2016.

Puente, I., González-Jorge, H., Martínez-Sánchez, J., Arias, P. 2013. Review of mobile mapping and surveying technologies. Measurement, 467, 2127-2145. doi:10.1016/j.measurement.2013.03.006

Razak, K. A., Santangelo, M., Van Westen, C. J., Straatsma, M. W., de Jong, S. M. 2013. Generating an optimal DTM from airborne laser scanning data for landslide mapping in a tropical forest environment. Geomorphology, 190, 112-125. doi:10.1016/j.geomorph.2013.02.021

Reitberger, J., Krzystek, P., Stilla, U. 2008. Analysis of full waveform LIDAR data for the classification of deciduous and coniferous trees. International Journal of Remote Sensing, 29(29), 1407-1431. doi:10.1080/01431160701736448

Reitberger, J., Schnörr, C., Krzystek, P., Stilla, U. 2009. 3D segmentation of single trees exploiting full waveform LIDAR data. ISPRS Journal of Photogrammetry and Remote Sensing, 64(6), 561-574. doi:10.1016/j.isprsjprs.2009.04.002

RIEGL, 2015. RIEGL VMX-450. http://www.riegl.com/uploads/tx_pxpriegldownloads/ DataSheet_VMX-450_2015-03- 19.pdf, Accessed 10 March 2016.

Roy, S., Byrne, J., Pickering, C. 2012. A systematic quantitative review of urban tree benefits, costs, and assessment methods across cities in different climatic zones. Urban Forestry and Urban Greening, 114, 351-363. doi:10.1016/j.ufug.2012.06.006

Saarinen, N., Vastaranta, M., Kankare, V., Tanhuanpää, T., Holopainen, M., Hyyppä, J., Hyyppä, H. 2014. Urban-tree-attribute update using multisource single-tree inventory. Forests, 5(5),1032-1052. doi:10.3390/f5051032

Sánchez-Lopera, J., Lerma, J. L. 2014. Classification of lidar bare-earth points, buildings, vegetation, and small objects based on region growing and angular classifier. International Journal of Remote Sensing, 35(19), 6955-6972. doi:10.1080/01431161.2014.960619

Schwarz, K. P., El-Sheimy, N. 2007. Digital mobile mapping systems-state of the art and future trends. In C. V. Tao, J. Li (Eds.), Advances in Mobile Mapping Technology pp. 3-19 Taylor and Francis/Balkema.

Shi, J., Malik, J. 2000. Normalized cuts and image segmentation. Pattern Analysis and Machine Intelligence, IEEE Transactions on, 22(8), 888-905. doi:10.1109/34.868688

Thaiutsa, B., Puangchit, L., Kjelgren, R., Arunpraparut, W. 2008. Urban green space, street tree and heritage large tree assessment in Bangkok, Thailand. Urban Forestry and Urban Greening, 73, 219-229. doi:10.1016/ j.ufug.2008.03.002

Topcon Positioning System. 2016. http://eijournal.com/print/articles/consider-the-benefits-of-mobile-lidar-for-transportation-projects, Accessed 10 May 2016.

Vainio, P., Tokola, T., Palander, T., Kangas, A. 2009. A GIS-based stand management system for estimating local energy wood supplies. Biomass and Bioenergy, 33(9), 1278-1288. doi:10.1016/j.biombioe.2009.05.021

Villari, C., Herms, D. A., Whitehill, J. G. A., Cipollini, D., Bonello, P. 2016. Progress and gaps in understanding mechanisms of ash tree resistance to emerald ash borer, a model for wood-boring insects that kill angiosperms. New Phytologist, 209(1), 63-79. doi:10.1111/nph.13604

Vosselman, G., Gorte, B., Sithole, G., Rabbani, T. 2004. Recognising structure in laser scanner point clouds. ISPRS Archives, 468, 4-6

Wang, L. 2016. Semi-automated generation of high-accuracy digital terrain models along roads using mobile laser scanning data. MSc Thesis, Department of Geography and Environmental Management, University of Waterloo.

Williams, K., Olsen, M. J., Roe, G. V., Glennie, C. 2013. Synthesis of transportation applications of mobile LiDAR. Remote Sensing, 5, 4652-4692. doi:10.3390/ rs5094652

Wolf, K. L., Bratton, N. 2006. Urban trees and traffic safety: Considering U.S. roadside policy and crash data. Arboriculture & Urban Forestry, 4(32), 170-179.

Wood, J. 1999. Tree inventories and GIS in urban forestry. Master in Forestry, Virginia Polytechnic Institute and State University.

Wu, F., Wen, C., Li, J., Wang, C. 2016. Automated extraction OF urban trees from mobile lidar point clouds. Proceedings of the 2nd ISPRS International Conference on Computer Vision in Remote Sensing, doi:10.1117/12.2234795.

Yao, W., Krzystek, P., Heurich, M. 2012. Tree species classification and estimation of stem volume and DBH based on single tree extraction by exploiting airborne full-waveform LiDAR data. Remote Sensing of Environment, 123, 368-380. doi:10.1016/ j.rse.2012.03.027

Yu, Y., Li, J., Guan, H., Wang, C., Yu, J. 2015a. Semi-automated extraction of street light poles from mobile LiDAR point-clouds. IEEE Transactions on Geoscience and Remote Sensing, 53(3), 1374-1386. doi:10.1109/TGRS.2014.2338915

Yu, Y, Li, J., Guan, H., Wang, C. 2015b. Automated extraction of urban road facilities using mobile laser scanning data. IEEE Transactions on Intelligent Transportation Systems, 16(4), 2167-2181. doi:10.1109/TITS.2015.2399492

Zhang, H. 2016. Rapid inspection of pavement markings using mobile laser scanning point clouds, MSc Thesis, Department of Geography and Environmental Management, University of Waterloo.